

Electronic Structure, mass fluctuation, and Localized Bond Properties of two-dimensional double-layer transition metal chalcogenide MX_2 ($\text{M} =$ Mo, W ; $\text{X} = \text{S, Se, Te}$) Calculated Based on Density Functional Theory and BBC model

Yaorui Tan and Maolin Bo*

Key Laboratory of Extraordinary Bond Engineering and Advanced Materials
Technology (EBEAM) of Chongqing, Yangtze Normal University, Chongqing 408100,
China

*Author to whom any correspondence should be addressed.
(E-mail addresses: bmlwd@yznu.edu.cn)

Abstract

This study systematically investigates the electronic structure and bonding properties of two-dimensional bilayer transition metal chalcogenides MX_2 ($\text{M} = \text{Mo, W}$; $\text{X} = \text{S, Se, Te}$) using density functional theory calculations. Through the analysis of band gaps, deformation bond energies, and non-Hermitian bonding characteristics of various MX_2 compounds, the electronic properties and chemical bonding features are comprehensively examined. The findings demonstrate that charge transfer plays a critical role in electron mass fluctuation, with the incorporation of topological geometric analysis confirming the influence of mass changes on atomic bonding and electronic states. Furthermore, Heterojunctions between distinct atomic layers are shown to effectively modulate the band gap of two-dimensional bilayer transition metal chalcogenides. This work establishes a theoretical foundation for advancing the application of these materials.

Keywords: Transition metal chalcogenide, Non-Hermitian bonding, Fluctuation of electron mass

1. Introduction

With the widespread application of two-dimensional materials in electronics, optics, and catalysis, transition metal chalcogenides MX_2 ($\text{M} = \text{Mo}, \text{W}$; $\text{X} = \text{S}, \text{Se}, \text{Te}$) have emerged as a focal point of research due to their unique physical and chemical properties. For instance, transition metal chalcogenide heterojunctions, utilized as electrode materials in lithium-ion batteries[1, 2], effectively enhance the structural stability and conductivity of the materials, significantly enhancing the specific capacity and cycling performance of the batteries. Additionally, materials such as molybdenum disulfide (MoS_2), with relatively large interlayer spacing, facilitate lithium-ion intercalation and deintercalation, demonstrating excellent performance in battery applications[3-5]. In addition, transition metal chalcogenide heterojunctions show great potential in photocatalysis[6-8], as they can promote water splitting to generate hydrogen and oxygen, achieving effective conversion of solar energy into chemical energy. Constructing heterojunctions enhances the separation efficiency of photogenerated charge carriers [9, 10], improving photocatalytic activity and offering innovative solutions for clean energy production. Furthermore, these materials are also used as light-absorbing layers in solar cells[11], where their tunable bandgap and excellent light absorption properties allow for the optimization of energy band structures, thereby improving the photovoltaic conversion efficiency. By varying the types of transition metals and chalcogen elements and adjusting the stacking of atomic layers, the bandgap of these materials can be precisely controlled, offering theoretical guidance for designing diverse optoelectronic devices[12-15]. Therefore, transition metal chalcogenide heterojunctions not only have significant applications in energy storage and optoelectronics but also offer vast prospects for the innovation and development of related technologies.

This study employs density functional theory (DFT) and the Binding Energy and Bond Charge (BBC) model[16] to analyze the band structure, density of states, and atomic bonding in two-dimensional bilayer MX_2 compounds. The band gaps of the heterostructures $\text{MoS}_2/\text{WSe}_2$, $\text{MoS}_2/\text{MoTe}_2$, and $\text{WSe}_2/\text{MoTe}_2$ [17-20] were determined to be 0.934 eV, 0.100 eV and 0.334 eV, respectively, while the band gaps of the bilayer WS_2 , WSe_2 , and WTe_2 [21-23] were 1.838 eV, 1.496 eV, and 0.917 eV. These findings underscore the significant variability in band gaps, emphasizing the capacity of interlayer heterostructures to modulate the bandgap of two-dimensional transition metal dichalcogenides. Furthermore, calculations of electron transfer and atomic

bonding demonstrate that charge transfer is intricately linked to electronic mass fluctuations, indicating that such variations profoundly influence atomic bonding and the overall electronic structure.

2. Methods

2.1 DFT calculations

The electronic properties and structural relaxation of MoS₂/WSe₂, MoS₂/MoTe₂, WSe₂/MoTe₂, WS₂, WSe₂, and WTe₂ were simulated using the Cambridge Sequential Total Energy Package (CASTEP). This package employs DFT with a plane wave pseudopotential and HSE06 to describe electron exchange and related potentials[24]. The calculations examined the energy, structure, bonding, and electronic properties of the aforementioned compounds: MoS₂/WSe₂, MoS₂/MoTe₂, WSe₂/MoTe₂, WS₂, WSe₂, and WTe₂. the TS scheme was applied for DFT-D dispersion correction to account for long-range vdW interactions. The cut-off energies, band gaps, and *k*-point grids utilized in this study are presented in **Table 1**. All structures were fully optimized without any symmetry constraints until the forces were reduced to less than 0.01 eV/Å, and the energy tolerance decreased below 5.0×10⁻⁶ eV the specified threshold per atom. For self-consistent field calculations, A convergence threshold 1.0×10⁻⁶ eV per atom was employed for MoS₂/WSe₂, MoS₂/MoTe₂, WSe₂/MoTe₂, WS₂, WSe₂, and WTe₂.

Table 1 Cut-off energies, bandgaps, and *k*-points of MoS₂/WSe₂, MoS₂/MoTe₂, WSe₂/MoTe₂, WS₂, WSe₂ and WTe₂

	Cut-off energy	<i>k</i> -point	Band gap (HSE06)
MoS ₂ /WSe ₂	650.0 eV	15×15×2	0.934 eV
MoS ₂ /MoTe ₂	650.0 eV	15×15×2	0.100 eV
WSe ₂ /MoTe ₂	650.0 eV	15×15×2	0.334 eV
WS ₂	650.0 eV	15×15×2	1.838 eV
WSe ₂	650.0 eV	15×15×2	1.496 eV
WTe ₂	650.0 eV	15×15×2	0.917 eV

2.2. BBC model

The BBC model[16] consists of the binding energy model (BC), bond charge model (BC), and the Hamiltonian of the BB model.

$$\begin{cases} H = \xi(0) \sum_I \hat{n}_I - J \sum_I \sum_{\rho} C_I^+ C_{I+\rho} = (E_n^a - \gamma^m A_n) \sum_I \hat{n}_I - J \sum_I \sum_{\rho} C_I^+ C_{I+\rho} \\ E_n(k) = E_n^a - \gamma^m A_n - J_n \sum_{\rho} e^{ik \cdot \bar{\rho}} \end{cases} \quad (1)$$

\hat{n}_I represents the electron number operator in the wanier representation. So, it

$\sum_l \hat{n}_l = C_l^+ C_l$ can be obtained. A_n represents the energy shift, E_n^a is the atomic energy level, and J is called the overlapping integral.

$$\begin{cases} A_n = -\int \phi^*(\vec{r}-\vec{l}) \left[V(\vec{r}) - v_a(\vec{r}-\vec{l}) \right] \phi(\vec{r}-\vec{l}) d\vec{r} \\ E_n^a = \int \phi^*(\vec{r}-\vec{l}) \left[-\frac{\hbar^2}{2m} \nabla^2 - v_a(\vec{r}-\vec{l}) \right] \phi(\vec{r}-\vec{l}) d\vec{r} \\ J_n = -\int \phi^*(\vec{r}) \left[V(\vec{r}) - v_a(\vec{r}-\vec{l}) \right] \phi(\vec{r}-\vec{l}) d\vec{r} \end{cases} \quad (2)$$

$\xi(0)$ is the local orbital electron energy. Therefore, there exists $\xi(0) = (E_n^a - A_n)$. E_n^a caused by the potential of $N-1$ atoms outside the lattice point l in

the lattice $V(r) = -\sum_{i,j,l_j \neq 0} \frac{1}{4\pi\epsilon_0} \frac{Z'e^2}{|\vec{r}_i - \vec{l}_j|}$ is the potential and $v_a(\vec{r}-\vec{l})$ is the atomic potential.

The binding energy (BE) shifts of the bulk and surface atoms can be expressed as:

$$\Delta E_v(B) = A_n, \quad \Delta E_v(i) = \gamma^m A_n \quad (3)$$

For chemical bonding, **Eq. 2** can be written as:

$$\gamma^m = \frac{E_v(i) - E_v(0)}{E_v(B) - E_v(0)} = \left(\frac{E_v(x) - E_v(0)}{E_v(B) - E_v(0)} \right)^m \approx \left(\frac{Z_x d_b}{Z_b d_x} \right)^m = \left(\frac{Z_b - \sigma'_i}{Z_b} \right)^m \left(\frac{d_x}{d_b} \right)^{-m} \approx \left(\frac{d_x}{d_b} \right)^{-m} \quad (4)$$

σ' is very small; therefore $(Z_b - \sigma')/Z_b \approx 1$, For metal $m =$

$$1, \left(\frac{Z_b - \sigma'_i}{Z_b} \right)^m \left(\frac{d_x}{d_b} \right)^{-m} = \left(\frac{d_x}{d_b} \right)^{-m'} \quad \text{obtain} \quad m' = m \left(1 - \frac{\ln \frac{Z_b - \sigma'_i}{Z_b}}{\ln \left(\frac{d_x}{d_b} \right)} \right). \quad \text{For example, we}$$

calculate the energy level shift of Mo $3d$, $E_v(B) = 227.569$ eV, $E_v(x) = 227.957$ eV,

$\frac{d_x}{d_b} = 0.875$; We use $E_i = -13.6 \frac{(Z - \sigma_i)^2}{n^2}$, considering the influence of angular

momentum $E_i(x) = -13.6 \frac{(Z - \sigma_i)^2}{(n + 0.7 * l)^2}$, $Z = 42$, $n = 3$, $l = 2$. For the orbital energy of

$$\text{Mo 3d: } E_{3d}(x) = -13.6 \frac{(42 - \sigma_i)^2}{(3 + 0.7 * 2)^2}, \quad \sigma_B = 24.001 \text{ eV}, \quad \sigma_x = 23.986 \text{ eV}, \quad \sigma'_i = 0.015,$$

$$m' = 0.995 \approx 1. \text{ Therefore } m \approx m'.$$

The Hamiltonian of a system in the BC model is expressed as (see supplemental material):

$$H = \sum_{k\sigma} \frac{\hbar^2 k^2}{2m} a_{k\sigma}^\dagger a_{k\sigma} + \frac{e_1^2}{2V} \sum_q^* \sum_{\bar{k}\sigma} \sum_{\bar{K}'\lambda} \frac{4\pi}{q^2} a_{\bar{k}+\bar{q},\sigma}^\dagger a_{\bar{K}'-\bar{q},\lambda}^\dagger a_{\bar{K}'\lambda} a_{\bar{k}\sigma} \quad (5)$$

The electron-interaction terms for density fluctuations is expressed as:

$$\begin{aligned} \Delta H &= H_{e1} - H_{e2} \\ &= \frac{e_1^2}{2V} \sum_q^* \sum_{\bar{k}\sigma} \sum_{\bar{K}'\lambda} \frac{4\pi}{q_1^2} a_{\bar{k}+\bar{q},\sigma}^\dagger a_{\bar{K}'-\bar{q},\lambda}^\dagger a_{\bar{K}'\lambda} a_{\bar{k}\sigma} - \frac{e_1^2}{2V} \sum_q^* \sum_{\bar{k}\sigma} \sum_{\bar{K}'\lambda} \frac{4\pi}{q_2^2} a_{\bar{k}+\bar{q},\sigma}^\dagger a_{\bar{K}'-\bar{q},\lambda}^\dagger a_{\bar{K}'\lambda} a_{\bar{k}\sigma} \\ &= \frac{1}{4\pi\epsilon_0} \sum_{i=1}^N \sum_{\substack{j=1 \\ i \neq j}}^N \frac{e^2}{2|\vec{r}_i - \vec{r}_j|} - \frac{1}{4\pi\epsilon_0} \sum_{i=1}^N \sum_{\substack{j=1 \\ i \neq j}}^N \frac{e^2}{2|\vec{r}_i' - \vec{r}_j'|} \end{aligned}$$

According to the charge conservation, for charge density fluctuations, the following formula:

$$\begin{aligned} \delta\hat{V}_{12} &= V_{e1} - V_{e2} \\ &= \sum_{i,j} \frac{1}{4\pi\epsilon_0} \frac{e^2}{2|\vec{r}_i - \vec{r}_j|} \int d^3\vec{r}_i \int d^3\vec{r}_j \rho(\vec{r}_i) \rho(\vec{r}_j) - \sum_{i,j} \frac{1}{4\pi\epsilon_0} \frac{e^2}{2|\vec{r}_i' - \vec{r}_j'|} \int d^3\vec{r}_i \int d^3\vec{r}_j' \rho(\vec{r}_i') \rho(\vec{r}_j') \\ &= \sum_{i,j} \frac{1}{4\pi\epsilon_0} \frac{e^2}{2|\vec{r} - \vec{r}'|} \int d^3r \int d^3r' \delta\rho(\vec{r}) \delta\rho(\vec{r}') \end{aligned} \quad (6)$$

The deformation bond energy δV_{bc} is represented by Equation 7:

$$\delta V_{bc} = \frac{1}{4\pi\epsilon_0} \frac{e^2}{2|\vec{r} - \vec{r}'|} \int d^3r \int d^3r' \delta\rho(\vec{r}) \delta\rho(\vec{r}') \quad (7)$$

Also, $\delta\rho$ satisfies the conditions outlined in Equation 8:

$$\left(\delta\rho_{\text{Hole-electron}} \leq \delta\rho_{\text{Antibonding-electron}} < \delta\rho_{\text{No charge transfer}} = 0 < \delta\rho_{\text{Nonbonding-electron}} \leq \delta\rho_{\text{Bonding-electron}} \right) \quad (8)$$

For atomic (strong) bonding states:

$$\delta\rho_{\text{Hole-electron}}(\vec{r}) \delta\rho_{\text{Bonding-electron}}(\vec{r}') < 0 (\text{Strong Bonding})$$

(9)

For atomic nonbonding or weak-bonding states:

$$\begin{cases} \delta\rho_{\text{Hole-electron}}(\vec{r})\delta\rho_{\text{Nonbonding-electron}}(\vec{r}') < 0(\text{Nonbonding or Weak Bonding}) \\ \delta\rho_{\text{Antibonding-electron}}(\vec{r})\delta\rho_{\text{Bonding-electron}}(\vec{r}') < 0(\text{Nonbonding or Weak Bonding}) \\ \delta\rho_{\text{Antibonding-electron}}(\vec{r})\delta\rho_{\text{Nonbonding-electron}}(\vec{r}') < 0(\text{Nonbonding}) \end{cases} \quad (10)$$

For atomic antibonding states:

$$\begin{cases} \delta\rho_{\text{Nonbonding-electron}}(\vec{r})\delta\rho_{\text{Bonding-electron}}(\vec{r}') > 0(\text{Antibonding}) \\ \delta\rho_{\text{Hole-electron}}(\vec{r})\delta\rho_{\text{Antibonding-electron}}(\vec{r}') > 0(\text{Antibonding}) \\ \delta\rho_{\text{Hole-electron}}(\vec{r})\delta\rho_{\text{Hole-electron}}(\vec{r}') > 0(\text{Antibonding}) \\ \delta\rho_{\text{Antibonding-electron}}(\vec{r})\delta\rho_{\text{Antibonding-electron}}(\vec{r}') > 0(\text{Antibonding}) \\ \delta\rho_{\text{Nonbonding-electron}}(\vec{r})\delta\rho_{\text{Nonbonding-electron}}(\vec{r}') > 0(\text{Antibonding}) \\ \delta\rho_{\text{Bonding-electron}}(\vec{r})\delta\rho_{\text{Bonding-electron}}(\vec{r}') > 0(\text{Antibonding}) \end{cases} \quad (11)$$

The formation of chemical bonds is related to fluctuations in electron density $\delta\rho$.

2.3 Riemann sphere and Möbius transformation

In Euclidean space R^3 , the complex number set C is represented as the XY -plane[25]. A sphere S is defined with center at $(0,0,1/2)$ and radius $1/2$, with the north pole $N = (0,0,1)$ as its vertex. The point $W = (X, Y, Z)$ lies on the surface of sphere S , and the line connecting N and W intersects the XY -plane at the projection point $w = x + iy$. Conversely, a line from the point $w = (x, y, 0)$ in the complex plane to N intersects the sphere at a unique point W . As shown in **Fig. 1**.

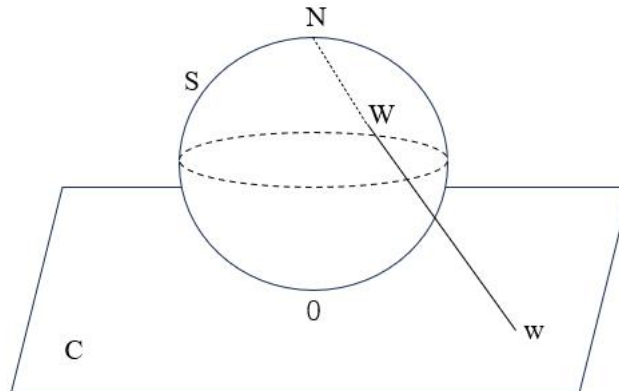


Fig. 1 Riemann sphere S and projection

This geometric explanation provides an objective representation of a point on a perforated spherical surface S and a complex plane. The analytical description of this

objective representation is as follows.

$$x = \frac{X}{1-Z}, \quad y = \frac{Y}{1-Z} \quad (12)$$

Substituting W with w :

$$Y = \frac{y}{x^2 + y^2 + 1}, \quad X = \frac{x}{x^2 + y^2 + 1}, \quad Z = \frac{x^2 + y^2}{x^2 + y^2 + 1} \quad (13)$$

The complex plane can cover the sphere, and a rational function defined on the extended complex plane can be viewed as a mapping of the sphere onto itself, transforming the pole into the north pole N . The Riemann sphere provides a powerful geometric framework for the relationship between the complex set and rational functions.

The Möbius transformation[26] maps a point z on the complex plane, expressed as $M(z) = \frac{az+b}{cz+d}$ with complex numbers a, b, c , and d (where $ad-bc \neq 0$). It is regarded as a fractional linear function that uniquely maps each point on the complex plane. Each Möbius transformation $M(z)$ corresponds to a (2×2) matrix, $[M]$, with complex elements:

$$M(z) = \frac{az+b}{cz+d} \rightarrow [M] = \begin{bmatrix} a & b \\ c & d \end{bmatrix} \quad (14)$$

To visualize the Möbius transformation $M(z) = \frac{az+b}{cz+d}$, we assume it has two fixed points ξ_- and consider it a mapping of itself $z \mapsto \omega = M(z)$, as shown in **Fig.**

2a.

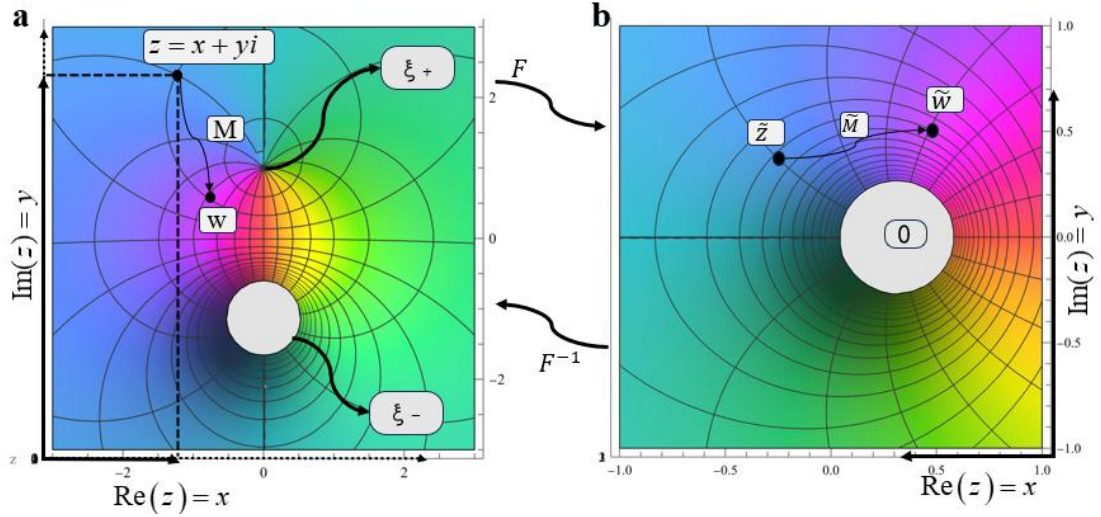


Fig. 2 Möbius transformation diagram

In the simplest Möbius transformation (see **Fig. 2a**), $F(z) = \frac{z - \xi_+}{z - \xi_-}$ the transformation maps one fixed point (set to ξ_+) to zero and the other fixed point (ξ_-) to ∞ infinity. **Fig. 2b** illustrates the image on the left under this Möbius transformation.

2.4 Lorenz transformation

Einstein discovered that there exists a spacetime interval Γ [27] between an observer and an event, such that the values of the spacetime interval seen by two observers are consistent. This spacetime interval Γ is defined by its square:

$$\Gamma^2 = T^2 - (X^2 + Y^2 + Z^2) = \tilde{T}^2 - (\tilde{X}^2 + \tilde{Y}^2 + \tilde{Z}^2) \quad (15)$$

Minkowski realized that this interval was a correct extension of the concept of distance, suitable for use in spacetime. The equidistant transformation and symmetry of spacetime maintain this interval's invariance. However, it is very different from the usual distance: the square of the interval between different events can be zero or even negative.

if two observers focus on the same photon, what they see is consistent, with each event along the photon's trajectory in spacetime having $\Gamma = 0$. This four-dimensional vector, which points to a specific light ray and has its "length" vanish, is called a zero vector.

The Lorentz transformation L is a linear transformation in spacetime, essentially a (4×4) matrix that maps an observer's observation (T, X, Y, Z) of an event to

another observer's observation $(\tilde{T}, \tilde{X}, \tilde{Y}, \tilde{Z})$ of the same event. In other words, L maintains a constant spatiotemporal distance, and the observations of two observers on the spatiotemporal interval of the same event are consistent.

Imagine an event O that generates an electric spark, emitting photons that propagate uniformly in all directions, forming a spherical surface centered at the origin. As time progresses, the radius of the spherical surface increases. At the time $T = 1$, the photon forms a sphere with a radius of 1, which is now represented by a Riemann sphere. Thus, it can be considered that the sphere composed of these photons consists of points marked with spacetime coordinates $(1, X, Y, Z)$, which can also be represented by complex numbers.

The projection formula $z = (z_1/z_2)$ onto the polar plane of the ball is given by:

$$X = \frac{\varsigma_1 \bar{\varsigma}_2 + \varsigma_2 \bar{\varsigma}_1}{|\varsigma_1|^2 + |\varsigma_2|^2}, Y = \frac{\varsigma_1 \bar{\varsigma}_2 - \varsigma_2 \bar{\varsigma}_1}{i(|\varsigma_1|^2 + |\varsigma_2|^2)}, Z = \frac{|\varsigma_1|^2 - |\varsigma_2|^2}{|\varsigma_1|^2 + |\varsigma_2|^2} \quad (16)$$

However, each beam of light is equivalent to any zero vector in the direction of that beam of light. If we let $T = 1$, we can choose a scalar factor $|\varsigma_1|^2 + |\varsigma_2|^2$ multiplied by the expression, which eliminates the denominator ($T = |\varsigma_1|^2 + |\varsigma_2|^2$). This new zero vector (T, X, Y, Z) (along the original spatiotemporal direction) can be represented as

$$\begin{aligned} T &= |\varsigma_1|^2 + |\varsigma_2|^2, \\ X &= \varsigma_1 \bar{\varsigma}_2 + \varsigma_2 \bar{\varsigma}_1, \\ Y &= -i(\varsigma_1 \bar{\varsigma}_2 - \varsigma_2 \bar{\varsigma}_1), \\ Z &= |\varsigma_1|^2 - |\varsigma_2|^2 \end{aligned} \quad (17)$$

It is straightforward to convert these formulas into the following form:

$$\begin{pmatrix} T+Z & X+iY \\ X-iY & T-Z \end{pmatrix} = 2 \begin{pmatrix} \varsigma_1 \bar{\varsigma}_1 & \varsigma_1 \bar{\varsigma}_2 \\ \varsigma_2 \bar{\varsigma}_1 & \varsigma_2 \bar{\varsigma}_2 \end{pmatrix} = 2 \begin{pmatrix} \varsigma_1 \\ \varsigma_2 \end{pmatrix} \begin{pmatrix} \bar{\varsigma}_1 & \bar{\varsigma}_2 \end{pmatrix} \quad (18)$$

which simplifies to:

$$\begin{pmatrix} T+Z & X+iY \\ X-iY & T-Z \end{pmatrix} = 2 \begin{pmatrix} \varsigma_1 \\ \varsigma_2 \end{pmatrix} \begin{pmatrix} \varsigma_1 \\ \varsigma_2 \end{pmatrix}^* \quad (19)$$

Here, the symbol “*” represents conjugate transposition. The spatiotemporal interval can now be succinctly represented as the determinant of this matrix:

$$\Gamma^2 = T^2 - (X^2 + Y^2 + Z^2) = \det \begin{pmatrix} T+Z & X+iY \\ X-iY & T-Z \end{pmatrix} \quad (20)$$

It is evident that this enlarged spatiotemporal vector is still a zero vector, as expected. The complex projection of the spherical polar plane has been utilized to represent the effect of the Möbius transformation $z \mapsto \tilde{z} = M(z)$ on this beam of light on the complex plane \mathbb{C} , as follows:

$$\begin{bmatrix} \varsigma_1 \\ \varsigma_2 \end{bmatrix} \mapsto \begin{bmatrix} \tilde{\varsigma}_1 \\ \tilde{\varsigma}_2 \end{bmatrix} = [M] \begin{bmatrix} \varsigma_1 \\ \varsigma_2 \end{bmatrix} \quad (21)$$

This results in a linear transformation of the zero vector generated by the light trajectory:

$$\begin{pmatrix} T+Z & X+iY \\ X-iY & T-Z \end{pmatrix} \mapsto \begin{pmatrix} \tilde{T}+\tilde{Z} & \tilde{X}+i\tilde{Y} \\ \tilde{X}-i\tilde{Y} & \tilde{T}-\tilde{Z} \end{pmatrix} = [M] \begin{pmatrix} T+Z & X+iY \\ X-iY & T-Z \end{pmatrix} [M]^* \quad (22)$$

Finally, imagine that this linear transformation applies to all spatiotemporal vectors (not just zero vectors). Since $\det[M] = 1 = \det[M]^*$, it can be concluded that this linear transformation preserves the spatiotemporal interval:

$$\tilde{\Gamma}^2 = \det \left\{ [M] \begin{pmatrix} T+Z & X+iY \\ X-iY & T-Z \end{pmatrix} [M]^* \right\} = \Gamma^2 \quad (23)$$

Each Möbius transformation on a complex plane \mathbb{C} corresponds to a unique Lorentz transformation in spacetime. Conversely, it can be proven that each Lorentz transformation corresponds to a unique Möbius transformation. Therefore, there exists a one-to-one correspondence between the Möbius transformation and the Lorentz transform, which reflects the invariance of spatiotemporal geometry in different reference frames.

2.5 Fluctuation of electron mass

The electron and positron can interact by exchanging a photon, and the photon can, in turn, transform into an electron-positron[28] pair. as shown in **Fig. 3**, the shaded region represents the vacuum polarization tensor, denoted as $i\Pi_{\mu\nu}(q)$. Based on infinitely many Feynman diagrams, as illustrated in **Fig. 4**, an approximation using the lowest-order diagram in **Fig. 3** with the vacuum polarization tensor leads to the diagram shown in **Fig. 5**.

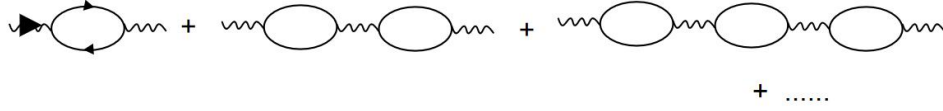


Fig. 3 the process of mutual annihilation

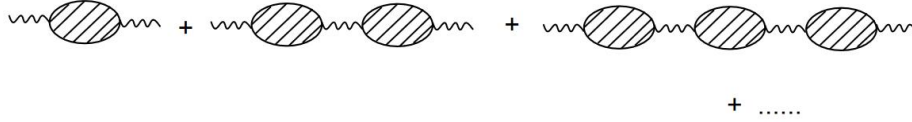


Fig. 4 physical photon propagation

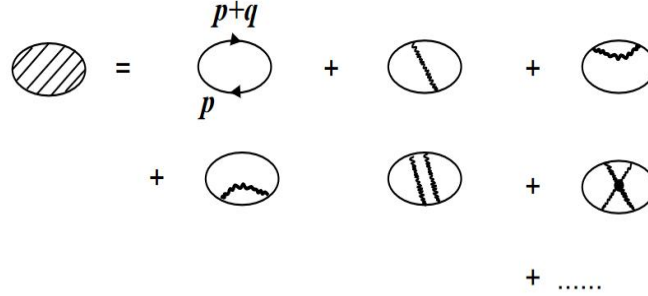


Fig. 5 infinite Feynman diagrams

The Lagrangian for this transformation $A \rightarrow (1/e)A$ is given by:

$$L = \bar{\psi} \left[i\gamma^\mu (\partial_\mu - iA_\mu) - m \right] \psi - \frac{1}{4e^2} F_{\mu\nu} F^{\mu\nu} \quad (24)$$

At $\psi \rightarrow e^{i\alpha}\psi$, $A_\mu \rightarrow A_\mu + \partial_\mu\alpha$ this point, the photon propagator taking the inverse of

$\frac{1}{4e^2} F_{\mu\nu} F^{\mu\nu}$ is proportional to e^2 :

$$iD_{\mu\nu}(q) = \frac{-ie^2}{q^2} \left(g_{\mu\nu} - (1-\xi) \frac{q_\mu q_\nu}{q^2} \right) \quad (25)$$

According to the combination of gauge -invariant diagrams and Lorentz invariance:

$$\begin{cases} q_\mu \Pi_{\mu\nu}(q) = 0 \\ \Pi_{\mu\nu}(q) = (q_\mu q_\nu - g_{\mu\nu} q^2) \Pi(q^2) \end{cases} \quad (26)$$

The physical photon propagation in **Fig. 4** is represented by the following geometric series:

$$\begin{aligned} iD_{\mu\nu}^P(q) &= iD_{\mu\nu}(q) + iD_{\mu\lambda}(q) i\Pi^{\lambda\rho}(q) iD_{\rho\nu}(q) \\ &\quad + iD_{\mu\lambda}(q) i\Pi^{\lambda\rho}(q) iD_{\rho\sigma}(q) i\Pi^{\sigma\kappa}(q) iD_{\kappa\nu}(q) + \dots \\ &= \frac{-ie^2}{q^2} g_{\mu\nu} \frac{1}{1 + e^2 \Pi(q^2)} + q_\mu q_\nu \end{aligned} \quad (27)$$

$$(1-\xi) \frac{q_\mu q_\nu}{q^2} \text{ in part } iD_{\mu\nu}(q) = \frac{-ie^2}{q^2} \left(g_{\mu\nu} - (1-\xi) \frac{q_\mu q_\nu}{q^2} \right) \text{ encounters } \Pi_{\lambda\rho}(q) \text{ as 0, in Eq.}$$

27, and the parameter ξ appears only in the $q_\mu q_\nu$ term and not in the physical amplitude, in **Eq. 26**.

The residue of the pole $iD_{\mu\nu}^P(q)$ is the square of the heavy positive charge, also known as physics:

$$e_R^2 = e^2 \frac{1}{1 + e^2 \Pi(0)} \quad (28)$$

Using Pauli-Villas regularization and integral convergence, we obtain:

$$i\Pi^{\mu\nu}(q) = (-) \int \frac{d^4 p}{(2\pi)^4} \frac{N_{\mu\nu}}{D} \quad (29)$$

Inside

$$N_{\mu\nu} = \text{tr}[\gamma_\nu (p + q + m) \gamma_\mu (p + m)] \quad (30)$$

$$\frac{1}{D} = \int_0^1 d\alpha \frac{1}{D} \quad (31)$$

Inside

$$\begin{cases} D = [l^2 + \alpha(1+\alpha)q^2 - m^2 + i\varepsilon]^2 \\ l = p + \alpha q \end{cases} \quad (32)$$

Finally, you can get:

$$\begin{aligned} \Pi_{\mu\nu}(q) = & -\frac{1}{2\pi^2} (q_\mu q_\nu - g_{\mu\nu} q^2) \int_0^1 d\alpha (1-\alpha) \\ & \cdot \left\{ \ln[m^2 - \alpha(1-\alpha)q^2] - \ln[m_\alpha^2 - \alpha(1-\alpha)q^2] \right\} \end{aligned} \quad (33)$$

We define:

$$\ln M^2 = \ln m_\alpha^2 \quad (34)$$

Then:

$$\Pi(q^2) = \frac{1}{2\pi^2} \int_0^1 d\alpha (1-\alpha) \ln \frac{M^2}{m^2 - \alpha(1-\alpha)q^2} \quad (35)$$

Summarizing **Eq. (28)** and **(35)**:

$$e_R^2 = e^2 \frac{1}{1 + \left[\frac{e^2}{12\pi^2} \right] \ln \left(\frac{M^2}{m^2} \right)} \simeq e^2 \left(1 - \frac{e^2}{12\pi^2} \ln \frac{M^2}{m^2} \right) \quad (36)$$

While M^2 representing the parameter of the ignorance bound, which confirms that the magnitude of the fluctuation mass of the charge is related to the imaginary mass M .

$$\Delta e^2 = \frac{e^2}{12\pi^2} \ln \frac{M^2}{m^2} \quad (37)$$

2.6 Principles of tropical geometry

Tropical geometry is a variant of algebraic geometry based on "Tropical Mathematics." In tropical geometry, the basic research object is the tropical semiring $(\mathbb{R} \cup \{\infty\}, \oplus, \odot)$ [29], and traditional operations such as addition and multiplication are replaced by "tropical addition" and "tropical multiplication":

$$x \oplus y = \min(x, y), \quad x \odot y = x + y$$

(38)

The curve defined by a polynomial equation is referred to as an algebraic curve. In traditional algebraic geometry, algebraic curves are described by solving equations; In tropical geometry, these curves are transformed into objects related to 'tropical addition' and 'tropical multiplication,' known as planar tropical curves. For polynomials with two variables:

$$p(x, y) = \bigoplus_{(i,j)} c_{ij} \odot x^i \odot y^j \quad (39)$$

The corresponding planar tropical curve $V(p)$ is the set of all points (x, y) satisfying this transformation. If p is a quadratic polynomial:

$p(x, y) = 1 \odot x^2 \oplus 1 \odot y^2 \oplus 2 \odot xy$ the corresponding tropical curve $V(p)$ forms a triangle with vertices at $(0,0)$, $(0,2)$, $(2,0)$:

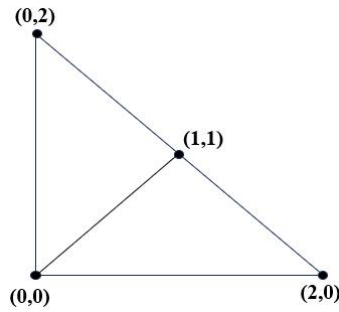


Fig. 6 Tropical geometry $V(1 \odot x^2 \oplus 1 \odot y^2 \oplus 2 \odot xy)$

A tropical matrix refers to a matrix whose elements are defined using tropical addition and multiplication operations. Unlike matrix operations in traditional linear algebra, tropical matrices adhere to the rules of tropical mathematics. When discussing eigenvalues of tropical matrices, the concept is analogous to eigenvalues in classical linear algebra but operates under tropical rules. Specifically, each quadratic polynomial can be associated with a (2×2) tropical matrix. For example, a

polynomial $f(x, y) = 2xy$ corresponds to a tropical matrix $A = \begin{bmatrix} 0 & 1 \\ 1 & 0 \end{bmatrix}$, see the

Supporting Materials. Similarly, for other forms of polynomials, such as $f(x, y) = x^2 + y^2 + 2xy$ or $f(x, y) = x^2 + y^2$, they can also be associated with tropical

matrices(Matrix of Quadratic Form) $A = \begin{bmatrix} 1 & 1 \\ 1 & 1 \end{bmatrix}$ and $A = \begin{bmatrix} 1 & 0 \\ 0 & 1 \end{bmatrix}$, respectively. Under this framework, tropical gradient maps can be constructed, showing the relationships and transformation rules between different polynomials and their corresponding tropical matrices:

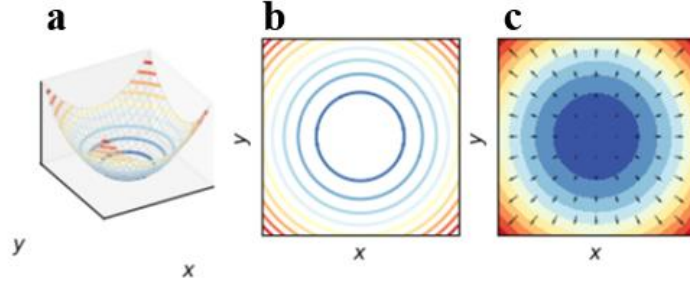


Fig. 7 Tropical geometry diagram

In **Fig. 7**, **a** presents the 3D surface plot of the quadratic polynomial, **b** shows the 2D contour plot of its function values, and **c** overlays the gradient field vectors on the 2D contour plot. This graph not only provides an intuitive visualization tool for understanding the structure of tropical matrices but also reveals the profound connection between polynomials and matrices in tropical algebra. Tropical geometry represents the equivalent mass in Schrödinger's equation. Lorentz transformation

In quantum mechanics, reduced mass is a parameter that describes the "effective" inertia exhibited by particles in certain systems[30]. Assuming we introduce the reduced mass effect in Schrödinger's equation, the reduced mass typically affects the energy spectrum of particles, especially in strong electric fields or non-uniform media. The definition of reduced mass \bar{M} is closely related to the relationship between potential energy and kinetic energy terms in the wave equation. The Hamiltonian operator is:

$$\hat{H} = -\frac{\hbar^2}{2m} \nabla^2 + U(\vec{r}) \quad (40)$$

The kinetic energy operator is $\hat{E}_k = -\frac{\hbar^2}{2m} \nabla^2$, where $\nabla^2 = \frac{\partial^2}{\partial x^2} + \frac{\partial^2}{\partial y^2} + \frac{\partial^2}{\partial z^2}$ is the Laplace operator. For the kinetic energy operator, multiply both sides by $\frac{1}{2}x^2$:

$$\frac{1}{2} \hat{E}_k x^2 = -\frac{\hbar^2}{2m} \nabla^2 \left(\frac{1}{2} x^2 \right) = -\frac{\hbar^2}{2m}$$

(41)

therefore:

$$\frac{1}{2}\hat{E}_k x_1^2 = -\frac{\hbar^2}{2m_1}, \frac{1}{2}\hat{E}_k x_2^2 = -\frac{\hbar^2}{2m_2} \quad (42)$$

let $x_1 = x, x_2 = y$, so we have:

$$\frac{1}{2}(\hat{E}_k x^2 + \hat{E}_k y^2) = -\frac{\hbar^2}{2m_x} - \frac{\hbar^2}{2m_y} = -\frac{\hbar^2}{2}\left(\frac{1}{m_x} + \frac{1}{m_y}\right) = -\frac{\hbar^2}{2}\left(\frac{m_x + m_y}{m_x m_y}\right) \quad (43)$$

further,

$$\hat{E}_k x^2 + \hat{E}_k y^2 = -\hbar^2 \left(\frac{m_x + m_y}{m_x m_y}\right) = -\hbar^2 \bar{M} \quad (44)$$

among them, \bar{M} is the equivalent mass, \hat{E}_k is the kinetic energy operator, and \hbar is the Planck constant. In this form, the reduced mass \bar{M} can be seen as a transformation result generated according to the rules of tropical geometry, representing how the effective mass of particles varies with the state of the system under different conditions. **Eq.43** satisfies the Lorentz transformation, see the Supporting Material.

Therefore, $-\hbar^2 \bar{M}$ can be represented in tropical geometry by the following formula:

$$f(x, y) = \hat{E}_k x^2 + \hat{E}_k y^2 \quad (45)$$

the corresponding tropical matrix is:

$$A = \begin{bmatrix} E_k & 0 \\ 0 & E_k \end{bmatrix} \quad (46)$$

When combining tropical geometry with the equivalent mass equation in Schrödinger's equation, we propose a way to re-characterize the equivalent mass through tropical operations. By representing the converted mass and potential energy terms as tropical polynomials, we can not only capture nonlinear effects in the system but also provide a new mathematical tool for complex systems in quantum mechanics.

Future research can further explore the application of tropical geometry in other physical models, especially in dealing with non-uniform and nonlinear quantum systems.

3.Results and discussion

3.1 Geometric structures

The two-dimensional bilayer MX_2 exhibits a typical layered structure, where M atoms and X atoms form a hexagonal arrangement through covalent bonds, and the two layers interact with each other through weak van der Waals forces. Geometric optimization was performed on the initial structures of the two-dimensional bilayer WS_2 , WSe_2 , WTe_2 , and heterojunctions $\text{MoS}_2/\text{WSe}_2$, $\text{MoS}_2/\text{MoTe}_2$, and $\text{WSe}_2/\text{MoTe}_2$. The optimized results are shown in **Fig. 8**. For different combinations of M (Mo, W) and X (S, Se, Te), variations in atomic radius and electronegativity can lead to variations in lattice constants and interlayer distances. The interlayer distances of $\text{MoS}_2/\text{WSe}_2$, $\text{MoS}_2/\text{MoTe}_2$, $\text{WSe}_2/\text{MoTe}_2$, WS_2 , WSe_2 and WTe_2 were found to be 3.837, 3.918, 3.895, 3.672, 3.740 and 3.900 Å. The changes in bond length and bond angle reflect the variations in the strength and geometric configuration of chemical bonds. Generally, the shorter the bond length, the stronger the chemical bond. From the calculation results, it can be seen that as the radius of X atom increases, the M-X bond length gradually increases, which is due to the increase in atomic size leading to an increase in interatomic distance. Although The change in bond angle is relatively small, it does exhibit certain patterns, which are related to the symmetry of the crystal structure and the interactions between atoms.

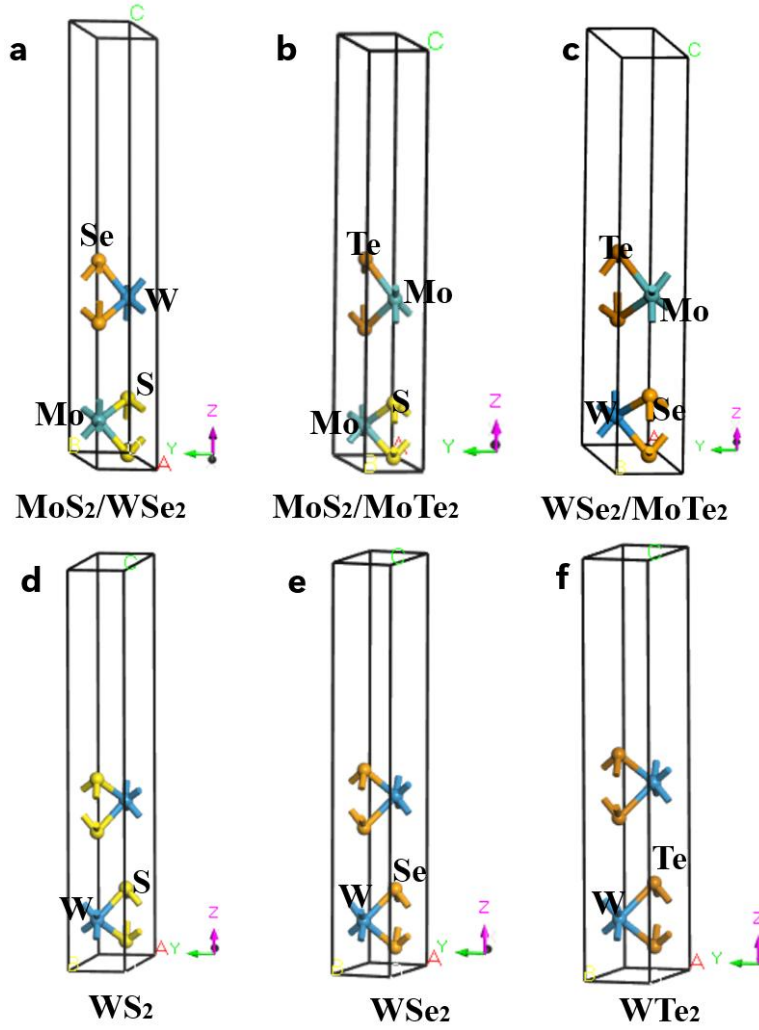


Fig. 8 Geometrical structures of (a) MoS₂/WSe₂, (b) MoS₂/MoTe₂, (c) WSe₂/MoTe₂, (d) WS₂, (e) WSe₂ and (f) WTe₂ and the lattice structure parameter sets are listed in **Table 2**.

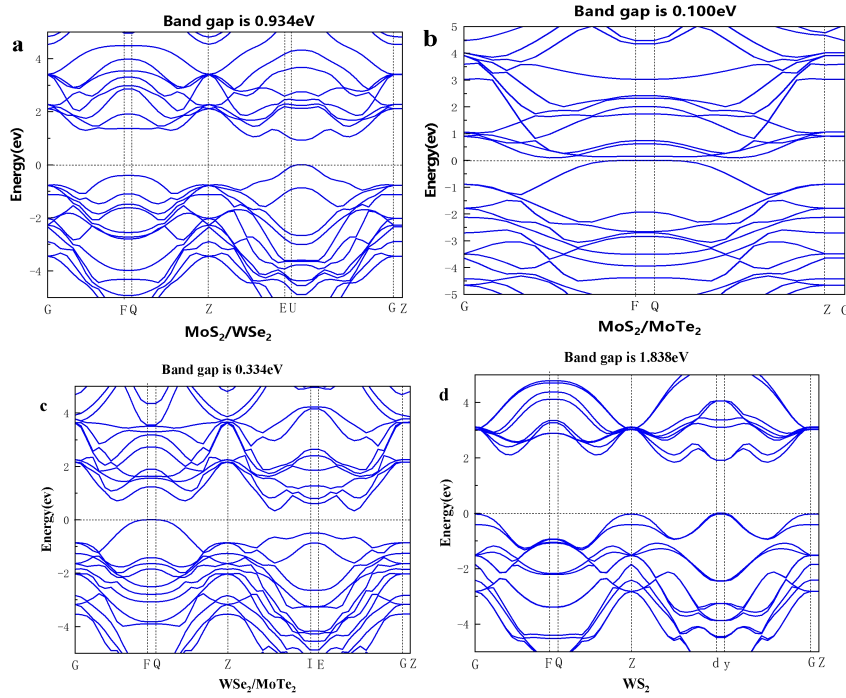
Table 2 Lattice and structural parameters of two-dimensional bilayer MX₂

	Interlayer distance (Å)	Lattice parameters (° / Å)						Bond length (Å)	Bond angle (°)
		α	β	γ	a	b	c		
MoS ₂ /WSe ₂	3.837	90	90	120	3.160	3.160	24.000	(Mo-S)	(S-Mo-S)
								2.408	81.425
								(W-Se)	(Se-W-Se)
MoS ₂ /MoTe ₂	3.918	90	90	60	3.160	3.160	24.000	2.522	87.389
								(Mo-S)	(S-Mo-S)
								2.408	81.432
WSe ₂ /MoTe ₂	3.895	90	90	60	3.282	3.282	24.000	(Mo-Te)	(Te-Mo-Te)
								2.699	94.948
								(W-Se)	(Se-W-Se)
WS ₂								2.542	83.587
								(Mo-Te)	(Te-Mo-Te)
								2.704	91.119

WS ₂	3.672	90	90	120	3.153	3.153	24.000	2.413	82.069
WSe ₂	3.740	90	90	120	3.282	3.282	24.000	2.542	83.588
WTe ₂	3.900	90	90	120	3.600	3.600	24.000	2.752	81.963

3.2 Band structure, local density of states (LDOS), deformation charge density, and electronic properties

The band structure of the two-dimensional bilayer MX₂ calculated using DFT is shown in **Fig. 9**. It can be observed that all compounds exhibit semiconductor properties, with bandgap widths varying within a certain range. Molecular dynamics simulation shows that the two-dimensional bilayer MX₂ is stable. The results are shown in the supplemental material. The bandgap width of MoS₂/WSe₂ is 0.934 eV, MoS₂/MoTe₂ is 0.100 eV, WSe₂/MoTe₂ is 0.334 eV, WS₂ is 1.838 eV, WSe₂ is 1.496 eV, and WTe₂ is 0.917 eV, respectively. From the shape of the band structure, the energy bands near the top of the valence band and the bottom of the conduction band exhibit different dispersion relations, reflecting the differences in the effective mass and motion characteristics of electrons in different directions.



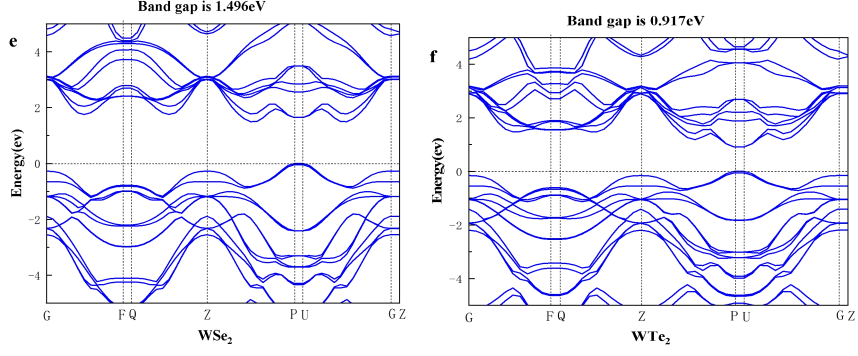


Fig. 9 Band structure of (a) MoS₂/WSe₂, (b) MoS₂/MoTe₂, (c) WSe₂/MoTe₂, (d) WS₂, (e) WSe₂ and (f) WTe₂.

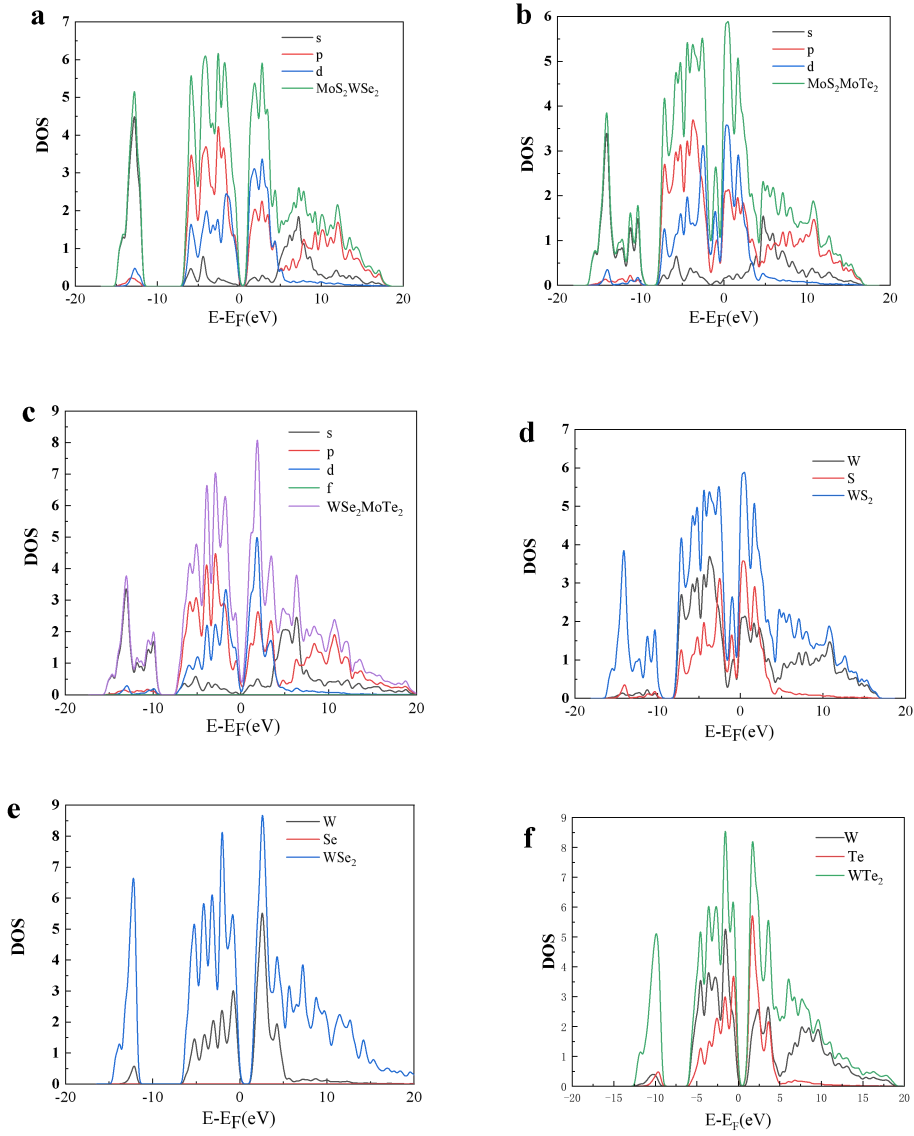


Fig. 10 density of states (DOS) of (a) MoS₂/WSe₂, (b) MoS₂/MoTe₂, (c) WSe₂/MoTe₂, (d) WS₂, (e) WSe₂ and (f) WTe₂

Fig. 10 shows the total DOS and PDOS of the two-dimensional bilayer MX₂.

From the total DOS, it can be seen that the main peaks of electron density distribution in the conductive band of MoS₂/WSe₂ heterojunction, MoS₂/MoTe₂ heterojunction, and WSe₂/MoTe₂ heterojunction are all in the negative energy direction, indicating that the structure is relatively stable. Near the Fermi level, the DOS is mainly contributed by the d orbitals of M and the p-orbitals of X. For Mo-based compounds, the d orbitals of Mo make a significant contribution in the lower energy region, while the p-orbitals of X are relatively prominent in the higher energy region. For W-based compounds, similar orbital contribution characteristics also exist, but due to the different atomic structure and electronic properties of W compared to Mo, the specific distribution of DOS varies. The DOS further reveals the details of the contribution of different atomic orbitals to electronic states, as well as their mutual hybridization. For example, in MoS₂, the $d_{x^2-y^2}$ and d_z orbitals of Mo have strong hybridization with the p_x and p_y orbitals of S within a certain energy range. This orbital hybridization has a significant impact on the formation of chemical bonds and the stability of electronic structures. The energy levels of two-dimensional bilayer WSe₂, WS₂, and WTe₂ intersect with one or more energy bands, indicating a high electron mobility. Therefore, these six types can be used as alternative materials for preparing electronic devices.

To analyze the electronic properties of the bonds, we used the deformation charge density (**Fig. 7**) of the Mo-S chemical bonds in MoS₂/WSe₂ (**Fig. 7a**)、 the Mo-Te chemical bonds in MoS₂/MoTe₂ (**Fig. 7b**)、 the W-Se chemical bonds in WSe₂/MoTe₂(**Fig. 7c**)、 the W-S chemical bonds in WS₂ **Fig. 7d**)、 the W-Se chemical bonds in WSe₂(**Fig. 7e**) and the W-Te chemical bonds in WTe₂ (**Fig. 7f**). The electron distributions are indicated by the color scale, where the blue and red areas represent an increase and decrease, respectively, in the number of electrons. The metal atoms of Te, S and Se is mainly displayed in blue, indicating a positive deformation charge density and the accumulation of a large amount of charge in this region of the structure. The W and Mo atoms are mainly displayed in red, indicating a negative deformation charge density and a large amount of charge divergence. It can be seen that the amount of charge transfer varies with the change of the X atom, which is related to the electronegativity of the X atom. X atoms with higher electronegativity attract more electrons, resulting in an increase in charge transfer. Meanwhile, due to its higher electronegativity, W atoms have a relatively smaller charge transfer amount

compared to Mo atoms when combined with the same X atom.

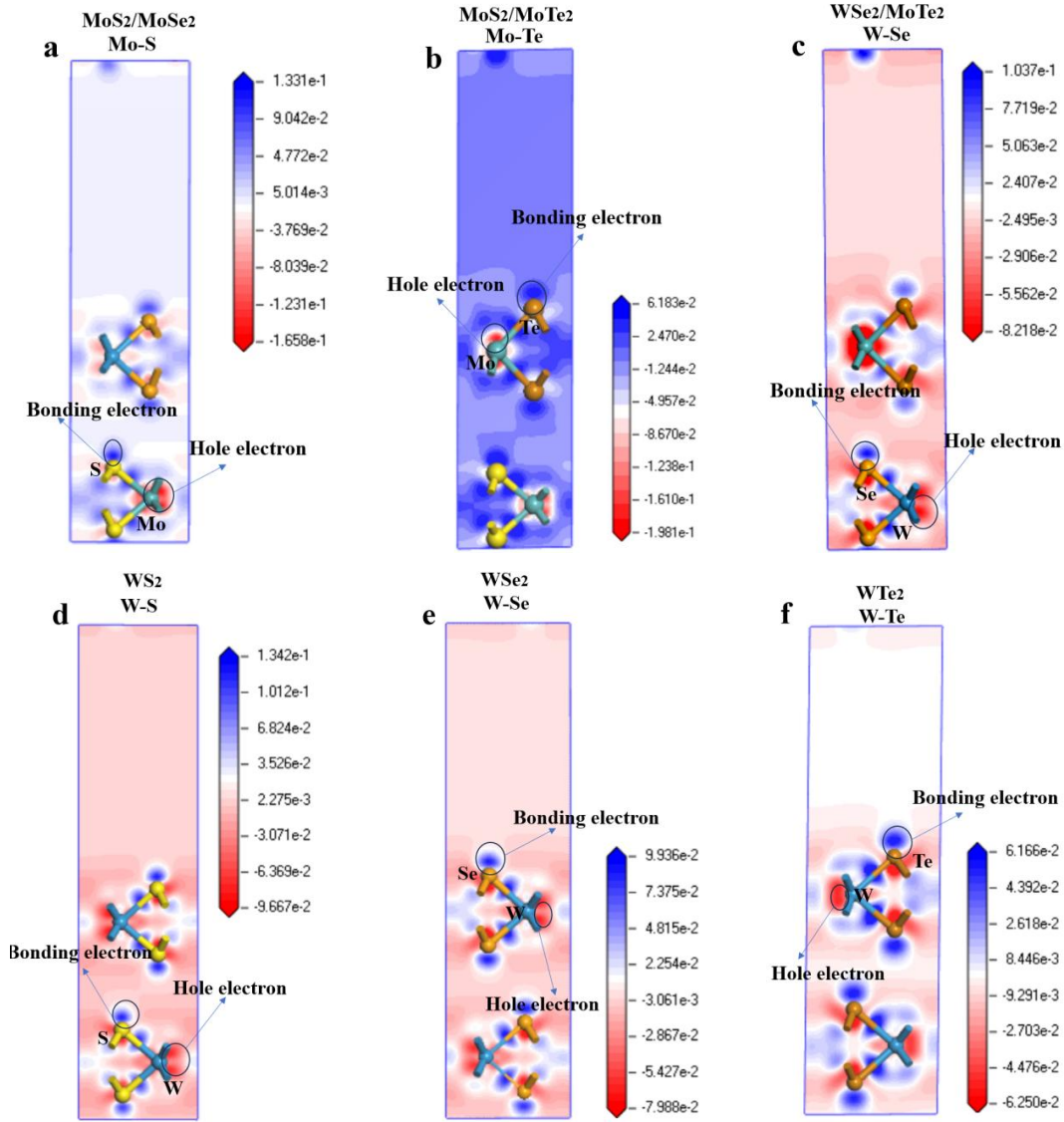


Fig. 11 Deformation charge densities of (a) MoS₂/WSe₂, (b) MoS₂/MoTe₂, (c) WSe₂/MoTe₂, (d) WS₂, (e) WSe₂ and (f) WTe₂

The established BBC model was used to convert the Hamiltonian values into bonding values (**Table 3**).

Table 3 Deformation charge density $\delta\rho(\vec{r}_{ij})$ and deformation bond energy

$\delta V_{bc}(\vec{r}_{ij})$, as obtained from the BBC model

$$(\varepsilon_0 = 8.85 \times 10^{-12} \text{ C}^2 \text{ N}^{-1} \text{ m}^{-2}, e = 1.60 \times 10^{-19} \text{ C}, |\vec{r}_{ij}| \approx d_{ij} / 2)$$

	MoS ₂ / WSe ₂	MoS ₂ / MoTe ₂	WSe ₂ / MoTe ₂	WS ₂	WSe ₂	WTe ₂
$r_{ij} (\text{ \AA })$	1.20 Mo-S	1.35 Mo-Te	1.27 W-Se	1.21 W-S	1.27 W-Se	1.38 W-Te

$r_i (\text{ \AA })$	1.05 (S)	1.38 (Te)	1.20 (Se)	1.05 (S)	1.20 (Se)	1.38 (Te)
$\vec{r}_j (\text{ \AA })$	1.54 (Mo)	1.54 (Mo)	1.62 (W)	1.62 (W)	1.62 (W)	1.62 (W)
$\delta\rho^{Bonding-electron}(\vec{r}_i)\left(\frac{e}{\text{ \AA }^3}\right)$	0.1331 (S)	0.0618 (Te)	0.1038 (Se)	0.1342 (S)	0.0994 (Se)	0.0676 (Te)
$\delta\rho^{Hole-electron}(\vec{r}_j)\left(\frac{e}{\text{ \AA }^3}\right)$	-0.1658 (Mo)	-0.1981 (Mo)	-0.0822 (W)	-0.0967 (W)	-0.0799 (W)	-0.0600 (W)
$\delta V_{bc}^{bonding}(\vec{r}_{ij})(\text{ eV })$	-0.5590	-0.6258	-0.3549	-0.3795	-0.3303	-0.2361
$\delta V_{bc}^{Antibonding}(\vec{r}_i)(\text{ eV })$	0.1626 (S)	0.1374 (Te)	0.1928 (Se)	0.1653 (S)	0.1768 (Se)	0.1644 (Te)
$\delta V_{bc}^{Antibonding}(\vec{r}_j)(\text{ eV })$	1.7120 (Mo)	2.444 (Mo)	0.5421 (W)	0.7502 (W)	0.5122 (W)	0.2888 (W)

The deformation charge density and electronic radius were used to calculate the deformation bond energies from **Eq. 7** as follows: -0.5590, -0.6258, -0.3549, -0.3795, -0.3303 and -0.2361 eV for Mo-S in MoS₂/WSe₂, Mo-Te in MoS₂/MoTe₂, W-Se in WSe₂/MoTe₂, W-S in WS₂, W-Se in WSe₂ and W-Te in WTe₂, respectively.

3.3 Non-Hermitian bonding of MoS₂/MoSe₂、MoS₂/MoTe₂、WSe₂/Mo-Te、WS₂、WSe₂ and WTe₂

$$M(z) = \frac{az+b}{cz+d} \rightarrow [M] = \begin{bmatrix} a & b \\ c & d \end{bmatrix} \quad (48)$$

The Möbius transform is a fractional linear function that maps point z on a complex plane to a unique point, where a, b, c , and d are plurals, and $ad - bc \neq 0$. To use **Eq. 11** for a point $W = (X, Y, Z)$ in real space, we first normalize the coordinates

$R_1(x_1, y_1, z_1)$ and $R_2(x_2, y_2, z_2)$ of two atoms in real space. The distance l between them is:

$$\sqrt{(x_1 - x_2)^2 + (y_1 - y_2)^2 + (z_1 - z_2)^2} = l \quad (49)$$

Therefore:

$$\sqrt{\frac{(x_1 - x_2)^2}{l^2} + \frac{(y_1 - y_2)^2}{l^2} + \frac{(z_1 - z_2)^2}{l^2}} = 1 \quad (50)$$

Order:

$$\begin{cases} X = \frac{x_1 - x_2}{l} \\ Y = \frac{y_1 - y_2}{l} \\ Z = \frac{z_1 - z_2}{l} \end{cases} \quad (51)$$

Point $W = (X, Y, Z)$ in real space satisfies $\sqrt{X^2 + Y^2 + Z^2} = 1$.

For a point w in the complex number set C , $w = x + iy$, $\text{Re}(w) = x$, and $\text{Im}(w) = y$.

As the projection point of W , w satisfies $x = \frac{X}{1-Z}$ or $y = \frac{Y}{1-Z}$. The projections of the atomic coordinates from real space onto a two-dimensional complex plane are listed in **Table 4**.

Table 4 Spatial coordinates of chemical bonds between MoS₂/WSe₂, MoS₂/MoTe₂, WSe₂/MoTe₂, WS₂, WSe₂ and WTe₂ and their projection points on the complex plane.

	Atom 1 (coordinates)	Atom 2 (coordinates)	X	Y	Z	W
MoS ₂ /WSe ₂	Mo (0.91,1.58,2.08)	S (1.82,0,3.65)	0.1430	0.4312	0.4258	0.2491+0.7509i
MoS ₂ /MoTe ₂	Mo (0.91,1.58,9.51)	Te (1.82,3.16,11.50)	0.1137	0.3427	0.5436	0.2491+0.7509i
WSe ₂ /MoTe ₂	W (1.91,3.30,2.22)	Se (0.96,1.65,3.91)	0.1393	0.4201	0.4407	0.2490+0.7510i
WS ₂	W (1.82,0,9.58)	S (0.91,1.58,11,17)	0.1415	0.4265	0.4320	0.2491+0.7509i
WSe ₂	W (1.90,0,10.04)	Se (0.95,1.63,11.74)	0.1399	0.4120	0.4481	0.2536+0.7464i
WTe ₂	W (2.08,0,10.85)	Te (1.04,1.80,12.65)	0.1430	0.4268	0.4285	0.2503+0.7497i

Based on **Eq. 49**, the projection points of Mo-S in MoS₂/WSe₂, Mo-Te in MoS₂/MoTe₂, W-Se in WSe₂/MoTe₂, W-S in WS₂, W-Se in WSe₂ and W-Te in WTe₂ in a two-dimensional complex plane are $0.2491 + 0.7509i$, $0.2491 + 0.7509i$, $0.2490 + 0.7510i$, $0.2491 + 0.7509i$, $0.2436 + 0.7464i$ and $0.2503 + 0.7497i$, respectively.

The elements of the matrix $\begin{bmatrix} a & b \\ c & d \end{bmatrix}$ in the Möbius transformation are complex

numbers. To determine the projection of chemical bond energy, according to **Table 4**, we define the bond energy coefficients V_{11} , V_{22} , and V_{12} as:

$$\begin{cases} V_{11} = \frac{1}{4\pi\epsilon_0} \frac{e^2}{2|\vec{r}_i|} \int d^3r \int d^3r \delta\rho^{Bonding-electron}(\vec{r}_i) \delta\rho^{Bonding-electron}(\vec{r}_i) = \delta V_{bc}^{Antibonding}(\vec{r}_i) \\ V_{22} = \frac{1}{4\pi\epsilon_0} \frac{e^2}{2|\vec{r}_j|} \int d^3r \int d^3r \delta\rho^{Hole-electron}(\vec{r}_j) \delta\rho^{Hole-electron}(\vec{r}_j) = \delta V_{bc}^{Antibonding}(\vec{r}_j) \\ V_{12} = \frac{1}{4\pi\epsilon_0} \frac{e^2}{2|\vec{r}_i - \vec{r}_j|} \int d^3r \int d^3r \delta\rho^{Bonding-electron}(\vec{r}_{ij}) \delta\rho^{Hole-electron}(\vec{r}_{ij}) = \delta V_{bc}^{bonding}(\vec{r}_{ij}) \end{cases} \quad (52)$$

Substituting **Eq. 49** and $Z=w=x+iy$ into the matrix elements of the Möbius transformation yields:

$$\begin{bmatrix} a & b \\ c & d \end{bmatrix} = \begin{bmatrix} V_{12}i & V_{11}i \\ V_{21}i & V_{22}i \end{bmatrix} \quad (53)$$

Substituting **Eq. 50** into **Eq. 48**, we obtain:

$$a = c = V_{12} = V_{21} = \delta V_{bc}^{bonding}(\vec{r}_{ij}), b = V_{11} = \delta V_{bc}^{Antibonding}(\vec{r}_i), d = V_{22} = \delta V_{bc}^{Antibonding}(\vec{r}_j) \quad (54)$$

Substituting **Eq. 51** into **Eq. 48** yields the Tan and Bo transformation[31] with the chemical bond energy as a coefficient:

$$F(z) = \frac{V_{12}iZ + V_{11}i}{V_{21}iZ + V_{22}i} \quad (55)$$

The chemical bond energy as a coefficient is used to determine the eigenvalues of the Hamiltonian energy, which are transformed into energy projections in the complex space through the Möbius transformation. The chemical bond energy coefficients are calculated by substituting **Eq. 49** into **Eq. 52** is substituted into **Eq. 55** to obtain the Möbius transformation of $\text{MoS}_2/\text{WSe}_2$, $\text{MoS}_2/\text{MoTe}_2$, $\text{WSe}_2/\text{MoTe}_2$, WS_2 , WSe_2 and WTe_2 .

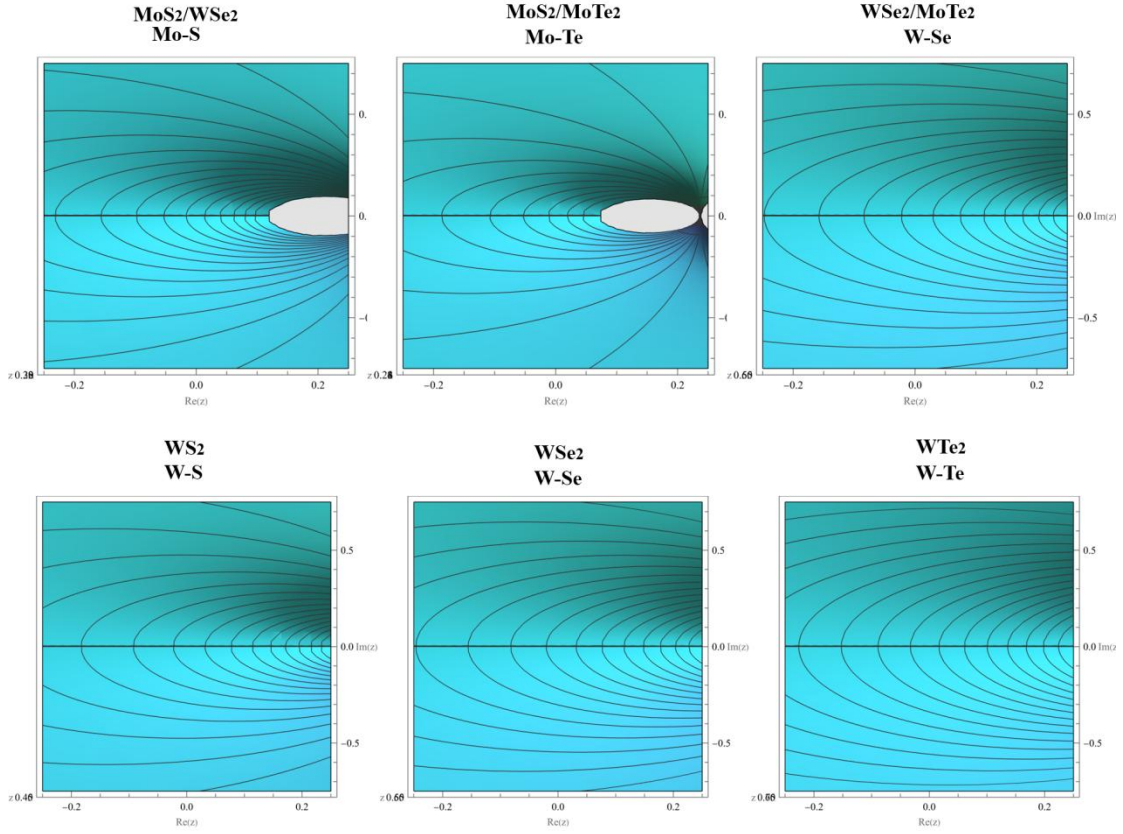


Fig. 12 Non-Hermitian chemical bond of MoS₂/WSe₂, MoS₂/MoTe₂, WSe₂/MoTe₂, WS₂, WSe₂ and WTe₂

The calculations using the $Z=w=x+iy$ function, illustrated in **Fig.12**, are as follows:

$$F(z) = \frac{-0.5590i \cdot w + 0.1626i}{-0.5590i \cdot w + 1.7120i}, \quad w = 0.25 + 0.75i \text{ of Mo-S in MoS}_2/\text{WSe}_2;$$

$$F(z) = \frac{-0.6258i \cdot w + 0.1374i}{-0.6258i \cdot w + 2.4440i}, \quad w = 0.25 + 0.75i \text{ of Mo-Te in MoS}_2/\text{MoTe}_2;$$

$$F(z) = \frac{-0.3549i \cdot w + 0.1928i}{-0.3549i \cdot w + 0.5421i}, \quad w = 0.25 + 0.75i \text{ of W-Se in WSe}_2/\text{MoTe}_2;$$

$$F(z) = \frac{-0.3795i \cdot w + 0.1653i}{-0.3795i \cdot w + 0.7502i}, \quad w = 0.25 + 0.75i \text{ of W-S in WS}_2;$$

$$F(z) = \frac{-0.3303i \cdot w + 0.1768i}{-0.3303i \cdot w + 0.5122i}, \quad w = 0.25 + 0.75i \text{ of W-Se in WSe}_2;$$

$$F(z) = \frac{-0.2361i \cdot w + 0.1644i}{-0.2361i \cdot w + 0.2888i}, \quad w = 0.25 + 0.75i \text{ of W-Te in WTe}_2.$$

3.4 Conformal transformation

Each $R(x+yi)$ can be represented in the following form:

$$R(x+yi) = P(x+yi)/Q(x+yi)$$

(56)

and

$$R(x + yi) = X + Yi,$$

$$R(x - yi) = X - Yi$$

$$(A + Bi)/(C + Di) = (A + Bi)(C - Di)/(C + Di)(C - Di) = \frac{AC + BD}{C^2 + D^2} + \frac{BC - AD}{C^2 + D^2}i \quad (57)$$

So $R(x + yi)$ can be expressed as:

$$R(x + yi) = \frac{A + Bi}{C + Di} = \frac{AC + BD}{C^2 + D^2} + \frac{BC - AD}{C^2 + D^2}i \quad (58)$$

Similarly, $R(x - yi)$ can be expressed as:

$$R(x - yi) = \frac{A - Bi}{C - Di} = \frac{AC + BD}{C^2 + D^2} - \frac{BC - AD}{C^2 + D^2}i \quad (59)$$

Therefore, every transformation can be represented as a complex number.

If A, B, C, and D are real numbers and measurable physical quantities, according to de Moivre theorem:

$$\begin{aligned} & r_1 (\cos \theta_1 + i \sin \theta_1) \times r_2 (\cos \theta_2 + i \sin \theta_2) \times \cdots \times r_n (\cos \theta_n + i \sin \theta_n) \\ &= r_1 r_2 \cdots r_n \{ \cos(\theta_1 + \theta_2 + \cdots + \theta_n) + i \sin(\theta_1 + \theta_2 + \cdots + \theta_n) \} \end{aligned} \quad (60)$$

where $r_1 = r_2 = \cdots = r_n = 1$, $\theta_1 = \theta_2 = \cdots = \theta_n = \theta$, obtain

$$(\cos \theta + i \sin \theta)^n = \cos n\theta + i \sin n\theta \quad (61)$$

where n is any positive integer, if $z = r(\cos \theta + i \sin \theta)$, then $1/z = (\cos \theta - i \sin \theta)/r$.

Another one

$$\begin{aligned} (\cos \theta + i \sin \theta)^{-n} &= (\cos \theta - i \sin \theta)^n \\ &= \{ \cos(-\theta) + i \sin(-\theta) \}^n \\ &= \cos(-n\theta) + i \sin(-n\theta) \end{aligned} \quad (62)$$

So, the de Moivre theorem holds for all positive or negative integer values of n .

Now let ABCD be the measurable value of energy, and based on the wave function $e^{i\theta} = \cos \theta + i \sin \theta$, we can directly convert the energy value into the form of a wave function:

$$\begin{aligned}
 r(\cos \theta + i \sin \theta) &= \begin{cases} \frac{A+Bi}{C+Di} = \frac{AC+BD}{C^2+D^2} + \frac{BC-AD}{C^2+D^2}i & (B > D) \\ \frac{A-Bi}{C-Di} = \frac{AC+BD}{C^2+D^2} - \frac{BC-AD}{C^2+D^2}i & (D > B) \end{cases} \\
 r(\cos \theta - i \sin \theta) &= \begin{cases} \frac{A+Bi}{C+Di} = \frac{AC+BD}{C^2+D^2} + \frac{BC-AD}{C^2+D^2}i & (D > B) \\ \frac{A-Bi}{C-Di} = \frac{AC+BD}{C^2+D^2} - \frac{BC-AD}{C^2+D^2}i & (B > D) \end{cases}
 \end{aligned} \tag{63}$$

Multiplying infinite amounts of energy (phase angle) into waveform for the same amount of energy

$$\begin{aligned}
 &\left(\frac{A+Bi}{C+Di}\right) \times \left(\frac{A+Bi}{C+Di}\right) \times \dots \times \left(\frac{A+Bi}{C+Di}\right) \\
 &= \left(\frac{AC+BD}{C^2+D^2} + \frac{BC-AD}{C^2+D^2}i\right)^n \\
 &= r^n (\cos \theta + i \sin \theta)^n \\
 &= r^n (\cos n\theta + i \sin n\theta) \\
 &= r^n e^{in\theta}
 \end{aligned} \tag{64}$$

For different energies

$$\begin{aligned}
 &\left(\frac{A_1+B_1i}{C_1+D_1i}\right) \times \left(\frac{A_2+B_2i}{C_2+D_2i}\right) \times \dots \times \left(\frac{A_k+B_ki}{C_k+D_ki}\right) \\
 &= \left(\frac{A_1C_1+B_1D_1}{C_1^2+D_1^2} + \frac{B_1C_1-A_1D_1}{C_1^2+D_1^2}i\right) \times \dots \times \left(\frac{A_kC_k+B_kD_k}{C_k^2+D_k^2} + \frac{B_kC_k-A_kD_k}{C_k^2+D_k^2}i\right) \\
 &= r_1 (\cos \theta_1 + i \sin \theta_1) \times r_2 (\cos \theta_2 + i \sin \theta_2) \times \dots \times r_k (\cos \theta_k + i \sin \theta_k) \\
 &= r_1 r_2 \dots r_k \{ \cos(\theta_1 + \theta_2 + \dots + \theta_k) + i \sin(\theta_1 + \theta_2 + \dots + \theta_k) \}
 \end{aligned} \tag{65}$$

Let ABCD be the measurable value of energy, based on the energy values calculated in **Table 3**, that is $B = \delta V_{bc}^{Antibonding}(\vec{r}_i)$, $D = \delta V_{bc}^{Antibonding}(\vec{r}_j)$,

$A = C = \delta V_{bc}^{bonding}(\vec{r}_{ij})$, for example, in the heterojunction MoS₂/WSe₂, $B = 0.1626$,

$D = 1.7120$, $A = C = -0.5590$ be substituted into **Eq. 63** :

$$\frac{A+Bi}{C+Di} = \frac{AC+BD}{C^2+D^2} + \frac{BC-AD}{C^2+D^2}i = 0.1822 + 0.2670i$$

Therefore, the measurable value of energy is represented as a complex number. Now, convert the energy value directly into the form of a wave function $r(\cos \theta + i \sin \theta) = re^{i\theta}$. The modulus r and radiation angle θ are calculated using the following formula:

$$r = \sqrt{x^2 + y^2}$$

$$\theta = \begin{cases} x > 0, \arctan(y/x) \\ x = 0, y > 0; \\ x = 0, y < 0; \\ x < 0, \arctan(y/x) + \pi \end{cases}$$

(66)

that is

$$0.1822 + 0.2670i = 0.3233(\cos 0.97 + i \sin 0.97)$$

Substitute into **Eq. 64**, the wave function $r^n e^{in\theta} = 0.3233^n (\cos 0.97n + i \sin 0.97n)$ can be obtained.

Now, substitute the energy values of six different substances, MoS₂/MoSe₂, MoS₂/MoTe₂, WSe₂/MoTe₂, WS₂, WSe₂, and WTe₂, into **Eq. 63** obtained:

$$\begin{cases} 0.1822 + 0.2670i = 0.3233(\cos 0.97 + i \sin 0.97) \\ 0.1143 + 0.2268i = 0.2540(\cos 1.10 + i \sin 1.10) \\ 0.5490 + 0.2953i = 0.6233(\cos 0.49 + i \sin 0.49) \\ 0.3792 + 0.3140i = 0.4924(\cos 0.69 + i \sin 0.69) \\ 0.5375 + 0.2982i = 0.6147(\cos 0.51 + i \sin 0.51) \\ 0.7418 + 0.2111i = 0.7713(\cos 0.28 + i \sin 0.28) \end{cases}$$

as shown in **Table 5**.

Table 5 The conformal transformation of energy obtains the argument θ_k and amplitude r_k of the wave function

	B	D	A=C	$\frac{AC+BD}{C^2+D^2} + \frac{BC-AD}{C^2+D^2}i$	θ (rad)	r
MoS ₂ /WSe ₂	0.1626	1.7120	-0.5590	$0.1822 + 0.2670i$	0.97	0.3233
MoS ₂ /MoTe ₂	0.1374	2.4440	-0.6258	$0.1143 + 0.2268i$	1.10	0.2540
WSe ₂ /MoTe ₂	0.1928	0.5421	-0.3549	$0.5490 + 0.2953i$	0.49	0.6233

WS ₂	0.1653	0.7502	-0.3795	0.3792 + 0.3140i	0.69	0.4924
WSe ₂	0.1768	0.5122	-0.3303	0.5375 + 0.2982i	0.51	0.6147
WTe ₂	0.1644	0.2888	-0.2361	0.7418 + 0.2111i	0.28	0.7713

3.5 Fluctuation of electron mass and reduced mass

3.5.1 Fluctuation of electron mass

From the Eq. 28 and Eq. 35 summary:

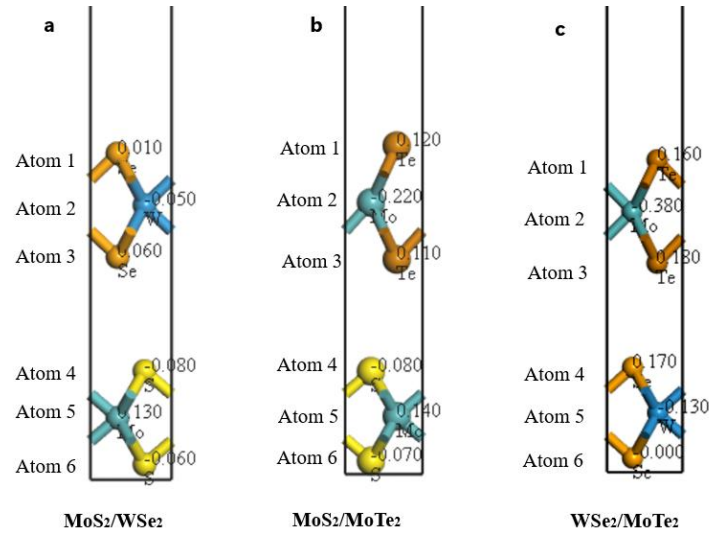
$$e_R^2 = e^2 \frac{1}{1 + \left[\frac{e^2}{12\pi^2} \right] \ln \left(\frac{M^2}{m^2} \right)} \approx e^2 \left(1 - \frac{e^2}{12\pi^2} \ln \frac{M^2}{m^2} \right)$$

While M^2 representing the parameter of the ignorance bound, which confirms that the magnitude of the fluctuation mass of the charge is related to the imaginary mass M .

$$\Delta e^2 = \frac{e^2}{12\pi^2} \ln \frac{M^2}{m^2}$$

Among them, electronic quality $m = 9.10956 \times 10^{-31} \text{kg}$

Fig. 13 shows the atomic positions, types, and corresponding charges of six two-dimensional bilayer structures



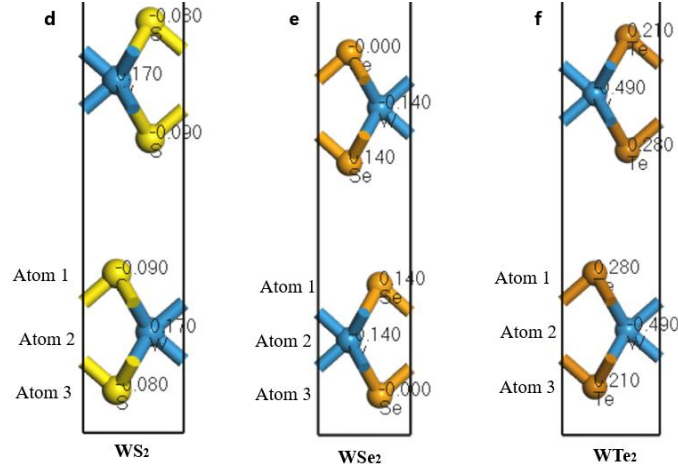


Fig. 13 Charge transfer of MoS₂/WSe₂, MoS₂/MoTe₂, WSe₂/MoTe₂, WS₂, WSe₂ and WTe₂

Based on **Fig. 13**, substitute the charges of each atom into **Eq. 37** to obtain the mass fluctuations of each atom, as shown in **Table 6**

Table 6 Fluctuation of electron mass M and charge transfer Δe

Structure	element	Δe	M
MoS ₂ /WSe ₂	Atom1	Se	0.010
	Atom2	W	-0.050
	Atom3	Se	0.060
	Atom4	S	-0.080
	Atom5	Mo	0.130
	Atom6	S	-0.060
MoS ₂ /MoTe ₂	Atom1	Te	0.120
	Atom2	Mo	-0.220
	Atom3	Te	0.110
	Atom4	S	-0.080
	Atom5	Mo	0.140
	Atom6	S	-0.070
WSe ₂ /MoTe ₂	Atom1	Te	0.160
	Atom2	Mo	-0.380
	Atom3	Te	0.180
	Atom4	Se	0.170
	Atom5	W	-0.130

	Atom6	Se	0	9.11E-31
	Atom1	S	-0.090	1.47E-30
WS ₂	Atom2	W	0.170	5.03E-30
	Atom3	S	-0.80	2.53E-14
	Atom1	Se	0.140	2.90E-30
WSe ₂	Atom2	W	-0.140	2.90E-30
	Atom3	Se	0	9.11E-31
	Atom1	Te	0.280	9.41E-29
WTe ₂	Atom2	W	-0.490	1.34E-24
	Atom3	Te	0.210	1.24E-29

3.5.2 Reduced mass of tropical geometry calculation

By combining tropical geometry with the reduced mass equation in Schrödinger's equation, we propose a way to re-characterize the reduced mass using tropical operations. Expressing the reduced mass $-\hbar^2\bar{M}$ and potential energy terms E_k as tropical polynomials:

$$f(x, y) = \hat{E}_k x^2 + \hat{E}_k y^2 \quad (67)$$

considering that the eigenvalues E_k of the corresponding tropical geometric matrix

$$A = \begin{bmatrix} E_k & 0 \\ 0 & E_k \end{bmatrix} \text{ correspond to chemical bonds } \delta V_{bc}^{bonding}(\vec{r}_{ij}), \text{ we have:}$$

$$E_k = \delta V_{bc}^{bonding}(\vec{r}_{ij})$$

Thus, the chemical bond Mo-S correspondence matrix in the heterojunction MoS₂/WSe₂ is:

$$A = \begin{bmatrix} -0.5590 & 0 \\ 0 & -0.5590 \end{bmatrix}$$

The tropical geometric quadratic polynomial corresponding to this (2×2) matrix is:

$$f(x, y) = -0.5590x^2 - 0.5590y^2 = \hbar^2\bar{M}$$

Similarly to MoS₂/MoTe₂, WSe₂/MoTe₂, WS₂, WSe₂ and WTe₂, a tropical gradient map can be further constructed to display the gradient relationship between

reduced mass $-\hbar^2 \bar{M}$, potential energy E_k , and their corresponding tropical matrices A , as shown in **Fig. 14**.

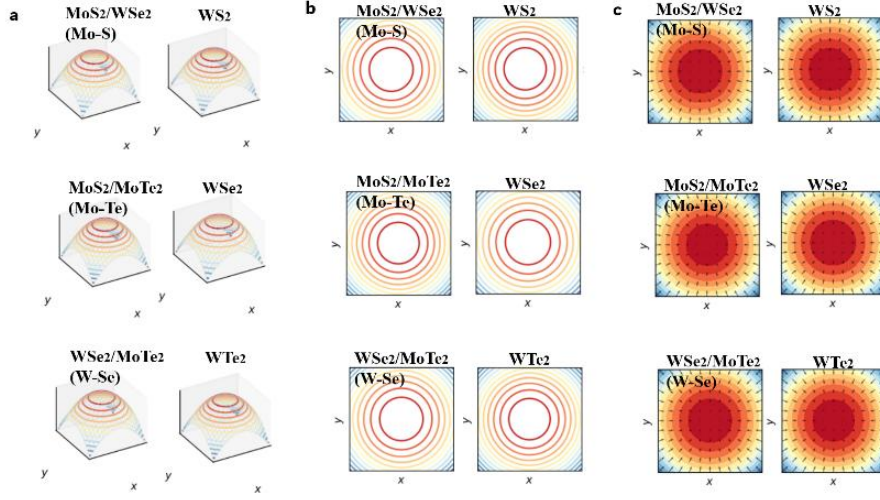


Fig. 14 Tropical gradient map of MoS₂/WSe₂, MoS₂/MoTe₂, WSe₂/MoTe₂, WS₂, WSe₂ and WTe₂

The 3D surface maps of the quadratic polynomials of six heterojunctions, illustrated in **Fig. 14 a**, are as follows: $f(x, y) = -0.5590x^2 - 0.5590y^2$ of Mo-S in MoS₂/WSe₂, $f(x, y) = -0.6258x^2 - 0.6258y^2$ of Mo-Te in MoS₂/MoTe₂, $f(x, y) = -0.3569x^2 - 0.3569y^2$ of W-Se in WSe₂/MoTe₂, $f(x, y) = -0.3795x^2 - 0.3795y^2$ of WS₂, $f(x, y) = -0.3303x^2 - 0.3303y^2$ of WSe₂, $f(x, y) = -0.2361x^2 - 0.2361y^2$ of WTe₂. The 2D contour plots of the function values of the quadratic polynomial, which are reduced mass $-\hbar^2 \bar{M}$ of the six heterojunctions, are shown in **Fig. 14 b**. **Fig. 14 c** depicts the vector of the gradient field based on the 2D contour map converted to reduced mass $-\hbar^2 \bar{M}$.

4. Conclusions

This study systematically investigates the electronic structure and chemical bonding properties of two-dimensional bilayer transition metal dichalcogenides (MX₂, M = Mo, W; X = S, Se, Te). Using DFT in conjunction with the BBC model, we analyze the effects of atomic bonding and electronic states, focusing on the band gaps, deformation binding energies, and non-Hermitian bonding characteristics of different MX₂ compounds. The results show that charge transfer plays a significant role in reduced mass fluctuations, and tropical geometry analysis further contributes to the reduced mass. The heterostructures formed by different atomic layers can effectively

modulate the band gap of the two-dimensional bilayer transition metal dichalcogenides. All compounds exhibit semiconductor properties, with band gaps varying within a certain range. The electronic band structure and DOS reflect the orbital characteristics and interactions of the electrons. The *d* orbitals of M and *p*-orbitals of X primarily contribute to the electronic states near the Fermi level, with orbital hybridization playing a crucial role in bond formation. This study provides a theoretical foundation for further exploration of these materials, especially in electronic devices and optoelectronic applications. Future research may focus on optimizing heterostructures and exploring the properties of other transition metal dichalcogenide systems.

References:

- [1] Y. Li, F. Wu, J. Qian, M. Zhang, Y. Yuan, Y. Bai, C. Wu, Metal chalcogenides with heterostructures for high - performance rechargeable batteries, *Small Science* 1 (2021) 2100012.
- [2] X. Liu, F. Xu, Z. Li, Z. Liu, W. Yang, Y. Zhang, H. Fan, H.Y. Yang, Design strategy for MXene and metal chalcogenides/oxides hybrids for supercapacitors, secondary batteries and electro/photocatalysis, *Coordination Chemistry Reviews* 464 (2022) 214544.
- [3] O. Samy, S. Zeng, M.D. Birowosuto, A. El Moutaouakil, A review on MoS₂ properties, synthesis, sensing applications and challenges, *Crystals* 11 (2021) 355.
- [4] Y. Tan, M. Bo, Electrostatic shielding effect and Binding energy shift of MoS₂, MoSe₂ and MoTe₂ materials, *arXiv preprint arXiv:2307.08035* (2023).
- [5] M. Bo, H. Li, Z. Huang, L. Li, C. Yao, Bond relaxation and electronic properties of two-dimensional Sb/MoSe₂ and Sb/MoTe₂ van der Waals heterostructures, *AIP Advances* 10 (2020).
- [6] M.U. Shahid, T. Najam, M.H. Helal, I. Hossain, S.M. El-Bahy, Z.M. El-Bahy, A. ur Rehman, S.S.A. Shah, M.A. Nazir, Transition metal chalcogenides and phosphides for photocatalytic H₂ generation via water splitting: a critical review, *International Journal of Hydrogen Energy* 62 (2024) 1113-1138.
- [7] D. Ge, R. Luo, X. Wang, L. Yang, W. Xiong, F. Wang, Internal and external electric field tunable electronic structures for photocatalytic water splitting: Janus transition-metal chalcogenides/C₃N₄ van der Waals heterojunctions, *Applied Surface Science* 566 (2021) 150639.
- [8] Y. Chen, Y. Wang, Z. Wang, Y. Gu, Y. Ye, X. Chai, J. Ye, Y. Chen, R. Xie, Y. Zhou, Unipolar barrier photodetectors based on van der Waals heterostructures, *Nature Electronics* 4 (2021) 357-363.
- [9] H. Yang, A short review on heterojunction photocatalysts: Carrier transfer behavior and photocatalytic mechanisms, *Materials Research Bulletin* 142 (2021) 111406.
- [10] F. Li, G. Zhu, J. Jiang, L. Yang, F. Deng, X. Li, A review of updated S-scheme heterojunction photocatalysts, *Journal of Materials Science & Technology* 177 (2024) 142-180.
- [11] Q. Xu, S. Wageh, A.A. Al-Ghamdi, X. Li, Design principle of S-scheme heterojunction photocatalyst, *Journal of Materials Science & Technology* 124 (2022) 171-173.
- [12] S. Wang, S. Zhao, X. Guo, G. Wang, 2D material - based heterostructures for rechargeable batteries, *Advanced Energy Materials* 12 (2022) 2100864.
- [13] D.M. Kennes, M. Claassen, L. Xian, A. Georges, A.J. Millis, J. Hone, C.R. Dean, D. Basov, A.N. Pasupathy, A. Rubio, Moiré heterostructures as a condensed-matter quantum simulator, *Nature Physics* 17 (2021) 155-163.
- [14] B. Huang, M.A. McGuire, A.F. May, D. Xiao, P. Jarillo-Herrero, X. Xu, Emergent phenomena and proximity effects in two-dimensional magnets and heterostructures, *Nature Materials* 19 (2020) 1276-1289.
- [15] H. Chen, S. Teale, B. Chen, Y. Hou, L. Grater, T. Zhu, K. Bertens, S.M. Park, H.R. Atapattu, Y. Gao, Quantum-size-tuned heterostructures enable efficient and stable inverted perovskite solar cells, *Nature Photonics* 16 (2022) 352-358.
- [16] L. Ge, M. Bo, Atomic bonding states of metal and semiconductor elements, *Physica Scripta*

98 (2023) 105908.

[17] J.E. Zimmermann, M. Axt, F. Mooshammer, P. Nagler, C. Schüller, T. Korn, U. Höfer, G. Mette, Ultrafast charge-transfer dynamics in twisted MoS₂/WSe₂ heterostructures, *ACS nano* 15 (2021) 14725-14731.

[18] Y. Balaji, Q. Smets, Á. Szabo, M. Mascaro, D. Lin, I. Asselberghs, I. Radu, M. Luisier, G. Groeseneken, MoS₂/MoTe₂ heterostructure tunnel FETs using gated Schottky contacts, *Advanced Functional Materials* 30 (2020) 1905970.

[19] S. Hussain, S.A. Patil, D. Vikraman, I. Rabani, A.A. Arbab, S.H. Jeong, H.-S. Kim, H. Choi, J. Jung, Enhanced electrocatalytic properties in MoS₂/MoTe₂ hybrid heterostructures for dye-sensitized solar cells, *Applied Surface Science* 504 (2020) 144401.

[20] J.F. Sierra, J. Fabian, R.K. Kawakami, S. Roche, S.O. Valenzuela, Van der Waals heterostructures for spintronics and opto-spintronics, *Nature Nanotechnology* 16 (2021) 856-868.

[21] Y. Li, J. Zhang, Q. Chen, X. Xia, M. Chen, Emerging of heterostructure materials in energy storage: a review, *Advanced Materials* 33 (2021) 2100855.

[22] P.V. Pham, S.C. Bodepudi, K. Shehzad, Y. Liu, Y. Xu, B. Yu, X. Duan, 2D heterostructures for ubiquitous electronics and optoelectronics: principles, opportunities, and challenges, *Chemical reviews* 122 (2022) 6514-6613.

[23] L. Pi, P. Wang, S.-J. Liang, P. Luo, H. Wang, D. Li, Z. Li, P. Chen, X. Zhou, F. Miao, Broadband convolutional processing using band-alignment-tunable heterostructures, *Nature Electronics* 5 (2022) 248-254.

[24] J. Heyd, G.E. Scuseria, M. Ernzerhof, Hybrid functionals based on a screened Coulomb potential, *The Journal of chemical physics* 118 (2003) 8207-8215.

[25] E.M. Stein, R. Shakarchi, *Complex analysis*, Princeton University Press 2010.

[26] R. Penrose, W. Rindler, *Spinors and space-time*, Cambridge university press 1984.

[27] T. Needham, *Visual complex analysis*, Oxford University Press 2023.

[28] A. Zee, *Quantum field theory in a nutshell*, Princeton university press 2010.

[29] D. Maclagan, B. Sturmfels, *Introduction to tropical geometry*, American Mathematical Society 2021.

[30] C. Kittel, P. McEuen, *Introduction to solid state physics*, John Wiley & Sons 2018.

[31] Y. Tan, M. Bo, Non - Hermitian Bonding and Electronic Reconfiguration of Ba₂ScNbO₆ and Ba₂LuNbO₆, *Annalen der Physik* (2024) 2400040.

Supplemental Material

Electronic Structure, mass fluctuation and Localized Bond Properties of two-dimensional double-layer transition metal chalcogenide MX_2 ($\text{M} = \text{Mo}, \text{W}$; $\text{X} = \text{S}, \text{Se}, \text{Te}$) Calculated Based on Density Functional Theory and BBC model

Yaorui Tan and Maolin Bo*

Key Laboratory of Extraordinary Bond Engineering and Advanced Materials

Technology (EBEAM) of Chongqing, Yangtze Normal University, Chongqing 408100, China

Corresponding Author: *E-mail: bmlwd@yznu.edu.cn (Maolin Bo)

Structural stability

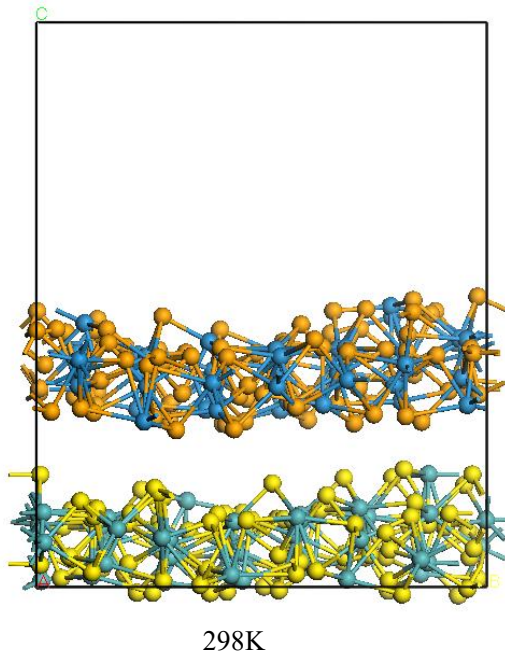
We used molecular dynamics (MD) to simulate the structural stability of two-dimensional double-layer transition metal chalcogenide MX_2 ($\text{M} = \text{Mo}, \text{W}$; $\text{X} = \text{S}, \text{Se}, \text{Te}$). The MX_2 structure were obtained by performing NVE ensemble with time increments at 1 fs for 100 ps (the total iteration steps are 100,000) until the potential energy accomplished a stable value. The box size and volume of two-dimensional double-layer transition metal chalcogenide MX_2 ($\text{M} = \text{Mo}, \text{W}$; $\text{X} = \text{S}, \text{Se}, \text{Te}$) structure, as is shown in the Table S1. The molecular dynamics simulation results show that the structures of two-dimensional double-layer transition metal chalcogenide MX_2 ($\text{M} = \text{Mo}, \text{W}$; $\text{X} = \text{S}, \text{Se}, \text{Te}$) are stable. The XRD diffraction patterns of two-dimensional double-layer transition metal chalcogenide MX_2 ($\text{M} = \text{Mo}, \text{W}$; $\text{X} = \text{S}, \text{Se}, \text{Te}$) MX_2 consistent with those in the database, so the crystal structure we constructed is reasonable.

Table S1 Box size and volume two-dimensional double-layer transition metal chalcogenide MX_2 ($\text{M} = \text{Mo}, \text{W}$; $\text{X} = \text{S}, \text{Se}, \text{Te}$)

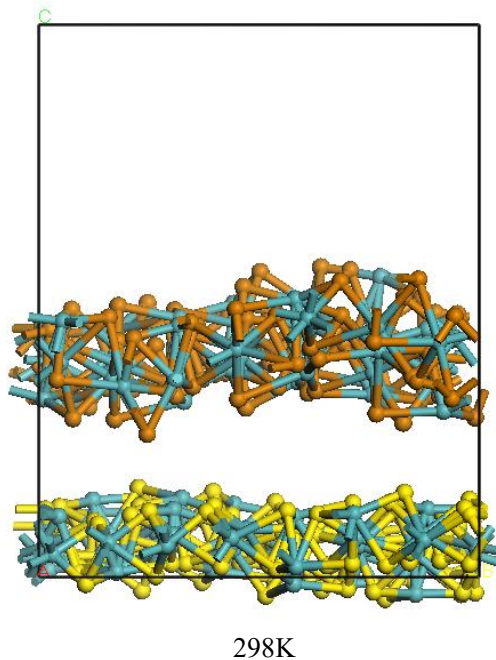
Structure	Volume	Box size			Angle		
		a(Å)	b(Å)	c(Å)	$\alpha(^{\circ})$	$\beta(^{\circ})$	$\gamma(^{\circ})$
$\text{MoS}_2/\text{WSe}_2$	10172.368 Å ³	22.1228	22.1228	24.000	90.000	90.000	120.000
$\text{MoS}_2/\text{MoTe}_2$	10172.368 Å ³	22.1228	22.1228	24.000	90.000	90.000	60.000
$\text{WSe}_2/\text{MoTe}_2$	10970.214 Å ³	22.974	22.974	24.000	90.000	90.000	60.000
WS_2	10126.071 Å ³	22.0724	22.0724	24.000	90.000	90.000	120.000
WSe_2	10970.214 Å ³	22.974	22.974	24.000	90.000	90.000	120.000
WTe_2	13199.058 Å ³	25.200	25.200	24.000	90.000	90.000	120.000

1. **Molecular dynamics (MD) to simulate the structural stability of two-dimensional double-layer transition metal chalcogenide MX_2 ($\text{M} = \text{Mo}, \text{W}$; $\text{X} = \text{S}, \text{Se}, \text{Te}$).**

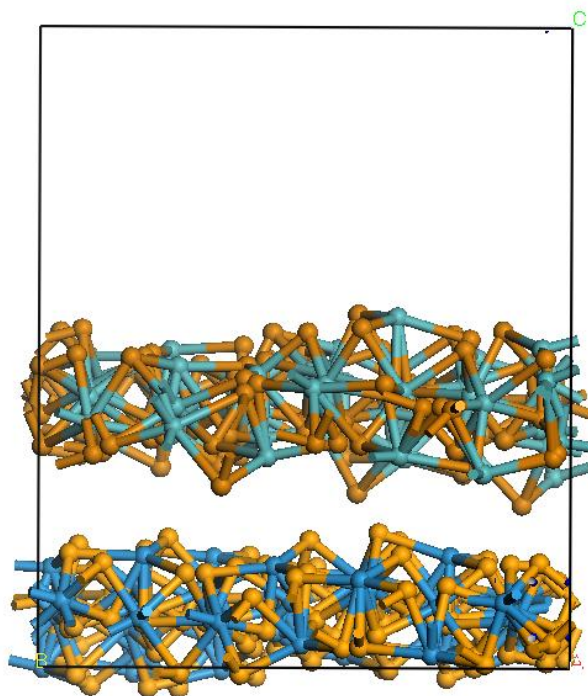
(1) **Structural stability of $\text{MoS}_2/\text{WSe}_2$**



(2) **Structural stability of $\text{MoS}_2/\text{MoTe}_2$**

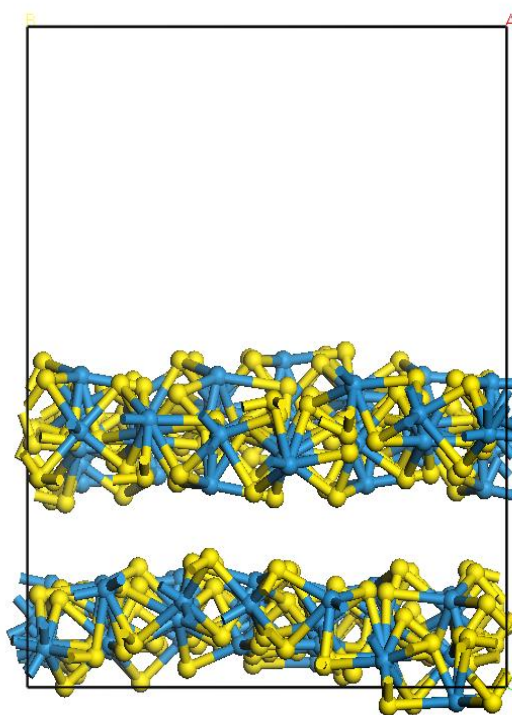


(3) **Structural stability of $\text{WSe}_2/\text{MoTe}_2$**



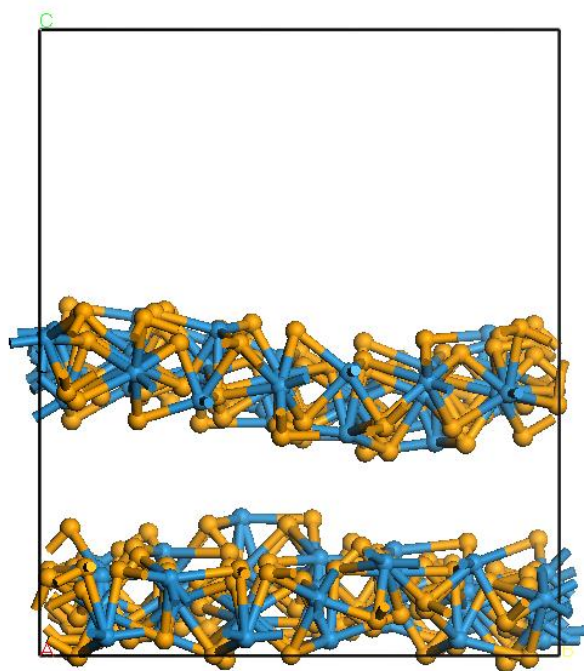
298K

(4) Structural stability of WS₂



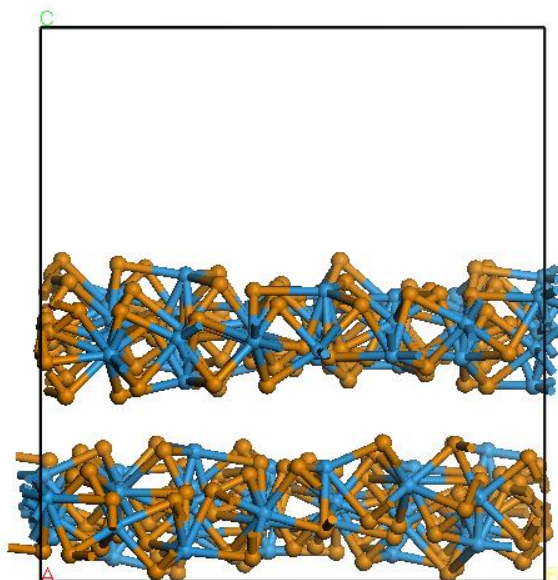
298K

(5) Structural stability of WSe₂



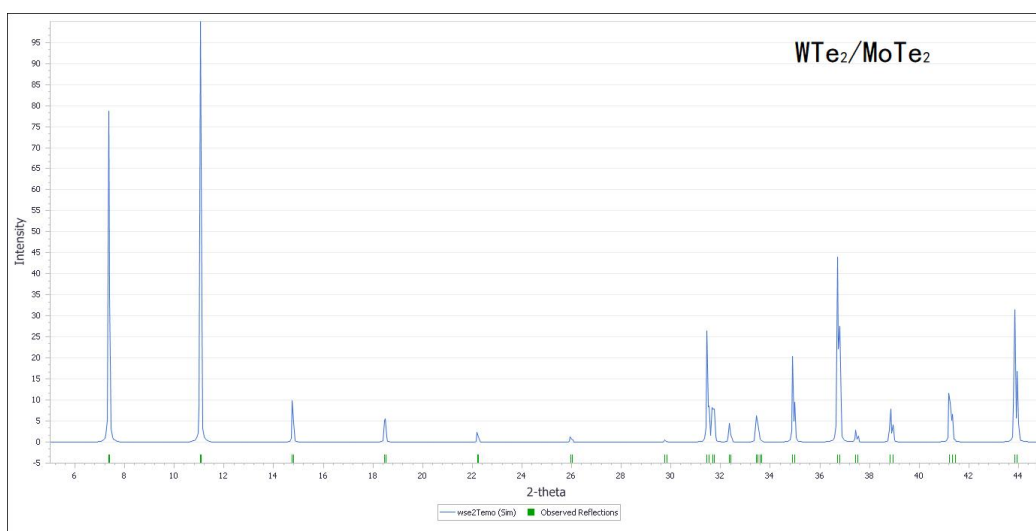
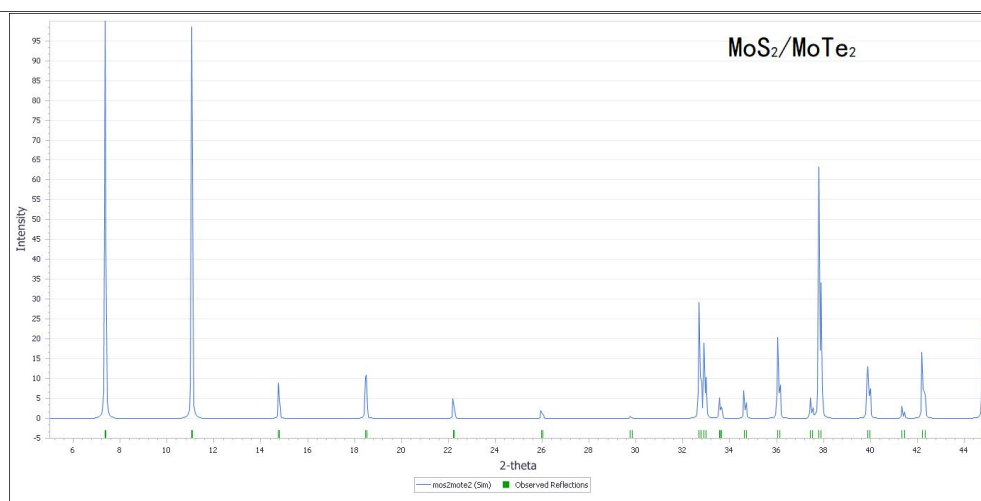
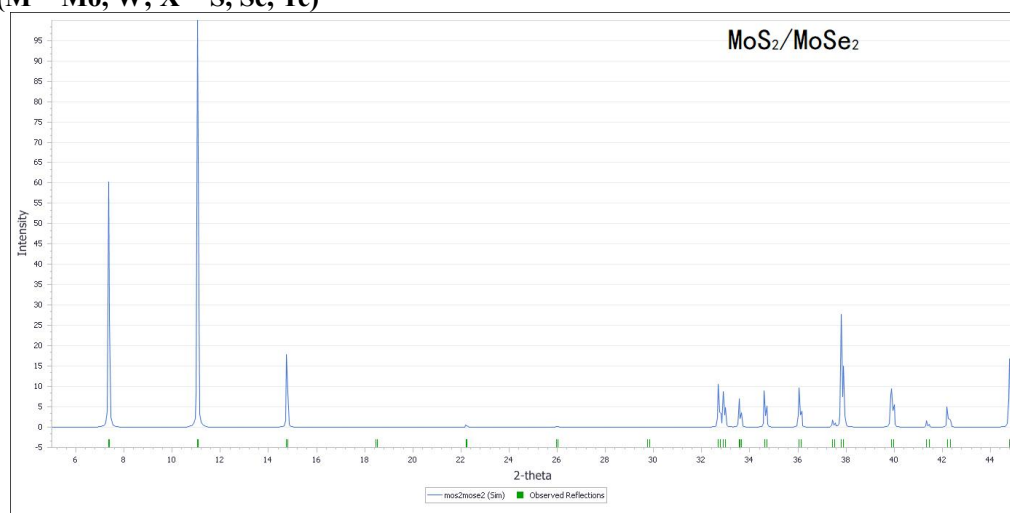
298K

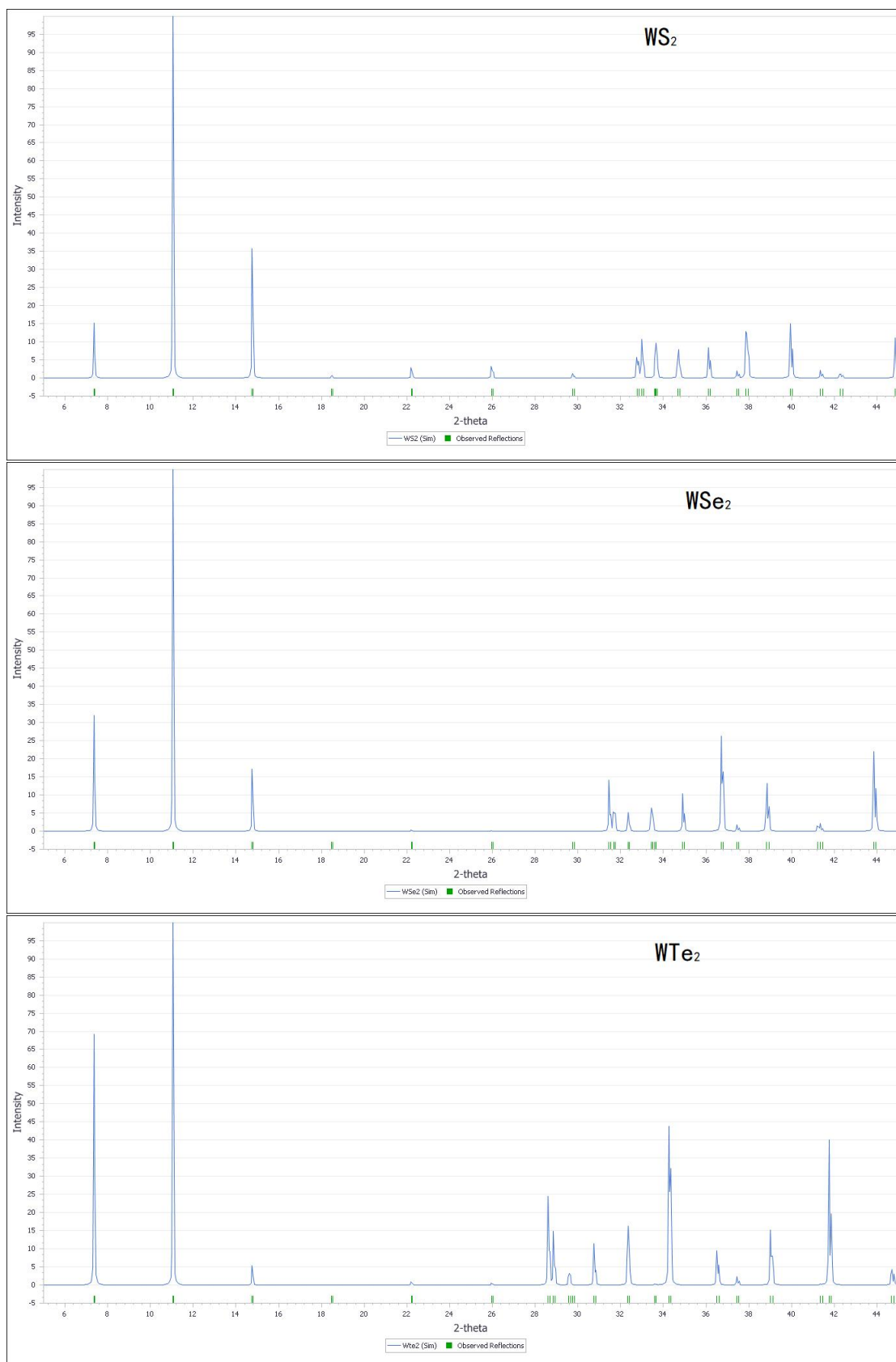
(6) Structural stability of WTe₂



298K

2.XRD diffraction patterns of two-dimensional double-layer transition metal chalcogenide MX_2 ($\text{M} = \text{Mo}, \text{W}$; $\text{X} = \text{S}, \text{Se}, \text{Te}$)





3. Lorentz transformation

According to special relativity, the laws of physics hold as well in a reference frame moving at a constant velocity as they do in a stationary frame. One embarrassing result is that it is impossible to distinguish which system (if any) is stationary, so it is impossible to know the "exact" speed of any other system.

According to the theory of special relativity, the laws of physics are equally valid in all inertial frames. An inertial frame is a system that follows Newton's first law of inertia: an object maintains a constant velocity in a straight line unless a force acts on it. It is easy to see that any two inertial frames must move at a constant speed relative to each other, and any frame that moves at a constant speed relative to an inertial frame is also an inertial system.

Assuming we have two inertial frames S and S' moving relative to S at a constant velocity V (magnitude V) (S therefore moves relative to S' at a velocity $-V$). We can also take the coordinates x/x' so that the motion follows the usual axis (see Figure 1), and place the clocks of each inertial frame at the origin, so that both clocks read zero when the two frames coincide (i.e. $x = x' = 0$, at that time $t = t' = 0$). Assuming that an event (x, y, z) occurs at time t in the S system.

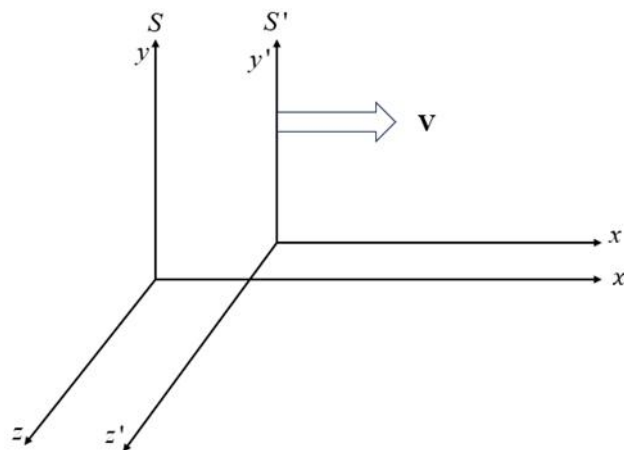


Figure 1

What are the spatiotemporal coordinates t' and (x', y', z') of the same event in the S' system? The answer is provided by the Lorentz transformation:

$$\begin{aligned}
x' &= \gamma(x - vt) \\
y' &= y \\
z' &= z \\
t' &= \gamma\left(t - \frac{v}{c^2}x\right)
\end{aligned}$$

among

$$\gamma \equiv \frac{1}{\sqrt{1 - \frac{v^2}{c^2}}}$$

The inverse exchange from S' to S can be easily changed. The symbol obtained is:

$$\begin{aligned}
x &= \gamma(x' - vt') \\
y &= y' \\
z &= z' \\
t &= \gamma\left(t' - \frac{v}{c^2}x'\right)
\end{aligned}$$

4. Four vectors

We define the position time four vectors x^μ , $\mu = 0, 1, 2, 3$ as follows:

$$x^0 = ct, x^1 = x, x^2 = y, x^3 = z$$

The Lorentz transformation can be written in a more symmetrical form:

$$\begin{aligned}
x^{0'} &= \gamma(x^0 - \beta x^1) \\
x^{1'} &= \gamma(x^1 - \beta x^0) \\
x^{2'} &= x^2 \\
x^{3'} &= x^3
\end{aligned}$$

among

$$\beta \equiv \frac{v}{c}$$

Tighter and more compact

$$x^{\mu'} = \sum_{\nu=0}^3 \Lambda_{\nu}^{\mu'} x^{\nu}, (\mu = 0, 1, 2, 3)$$

The coefficient $\Lambda_{\nu}^{\mu'}$ can be seen as a matrix element of a matrix Λ :

$$\Lambda = \begin{pmatrix} \gamma & -\gamma\beta & 0 & 0 \\ -\gamma\beta & \gamma & 0 & 0 \\ 0 & 0 & 1 & 0 \\ 0 & 0 & 0 & 1 \end{pmatrix}$$

(i.e $\Lambda_0^0 = \Lambda_1^1 = \gamma$; $\Lambda_0^1 = \Lambda_1^0 = -\gamma\beta$; $\Lambda_2^2 = \Lambda_3^3 = 1$; all others are 0). To avoid writing too many summation signs, we will use Einstein's "summation rule", which requires automatic summation of repeated Greek indices (one subscript, one superscript) from 0 to 3. Therefore, the equation is written as follows at the end:

$$x^{\mu'} = \Lambda_{\nu}^{\mu'} x^{\nu}$$

The special advantage of this neat expression is that it has the same form for Lorentz transformations that are not along the x -direction; In fact, the coordinate axes of S and S' do not even need to be parallel to each other; The matrix Λ is naturally more complex, but equation still holds.

When transitioning from S to S' , although the individual coordinates of the event may change, a special combination of them remains unchanged:

$$I = (x^0)^2 - (x^1)^2 - (x^2)^2 - (x^3)^2 = (x^{0'})^2 - (x^{1'})^2 - (x^{2'})^2 - (x^{3'})^2$$

The quantity that has the same value in any inertial frame is called an invariant.

Similarly, if an appropriate angle θ is chosen as the pivot (counterclockwise pivot):

$$\begin{cases} x \rightarrow x \cos \theta + y \sin \theta \\ y \rightarrow -x \sin \theta + y \cos \theta \end{cases}$$

Represent by matrix

$$\begin{pmatrix} x \\ y \end{pmatrix} \rightarrow \begin{pmatrix} x \cos \theta + y \sin \theta \\ -x \sin \theta + y \cos \theta \end{pmatrix} = \begin{pmatrix} \cos \theta & \sin \theta \\ -\sin \theta & \cos \theta \end{pmatrix} \begin{pmatrix} x \\ y \end{pmatrix}$$

Represent by matrix components

$$x'_i = R_i^j x_j, \quad x_i = \begin{pmatrix} x \\ y \end{pmatrix}, \quad i, j = 1, 2$$

Take transpose

$$(x' \ y') = (x \ y) \begin{pmatrix} \cos \theta & -\sin \theta \\ \sin \theta & \cos \theta \end{pmatrix}$$

$$x'^i = x^j (R^T)_j^i, \quad x^j = (x \ y), \quad i, j = 1, 2, \quad R_i^j x_j = R_i^1 x_1 + R_i^2 x_2$$

therefore

$$\begin{aligned} R^T R &= \begin{pmatrix} \cos \theta & -\sin \theta \\ \sin \theta & \cos \theta \end{pmatrix} \begin{pmatrix} \cos \theta & \sin \theta \\ -\sin \theta & \cos \theta \end{pmatrix} \\ &= \begin{pmatrix} \cos^2 \theta + \sin^2 \theta & \cos \theta \sin \theta - \sin \theta \cos \theta \\ \sin \theta \cos \theta - \cos \theta \sin \theta & \cos^2 \theta + \sin^2 \theta \end{pmatrix} \\ &= \begin{pmatrix} 1 & 0 \\ 0 & 1 \end{pmatrix} = I \end{aligned}$$

So $r^2 = x^2 + y^2 + z^2$ remains constant under rotation.

Now, I want to write this invariant in the form of summation: $\sum_{\mu=0}^3 x^{\mu} x^{\mu}$, but

unfortunately there are three repeated negative signs for summation. To preserve their traces, we introduce a metric $g_{\mu\nu}$ whose components can be displayed as a matrix g :

$$g = \begin{pmatrix} 1 & 0 & 0 & 0 \\ 0 & -1 & 0 & 0 \\ 0 & 0 & -1 & 0 \\ 0 & 0 & 0 & -1 \end{pmatrix}$$

(i.e. $g_{00} = 1; g_{11} = g_{22} = g_{33} = -1$, all others are 0). With the help of $g_{\mu\nu}$, invariants I can be written in the form of double sums:

$$I = \sum_{\mu=0}^3 \sum_{\nu=0}^3 g_{\mu\nu} x^\mu x^\nu = g_{\mu\nu} x^\mu x^\nu$$

Furthermore, we define covariant four vectors x_μ (with indicators listed below) as follows:

$$x_\mu \equiv g_{\mu\nu} x^\nu$$

(That is, $x_0 = x^0, x_1 = -x^1, x_2 = -x^2, x_3 = -x^3$). To emphasize the difference, we call the "original" four vector x^μ (with the index above) the inverted four vector. Invariants can therefore be written in the simplest form:

$$I = x^\mu x_\mu$$

(Or equivalently written $x_\mu x^\mu$). Once you get used to this method, it will become very simple. (Furthermore, it effectively extends non-Cartesian coordinate systems to the curved spaces encountered in general relativity, although neither of these things are relevant to us here.)

Bit-time four vectors x^μ are typical of all four vectors. When we change from one inertial space to another, we define four vectors a^μ as a four component quantity to transform in the same way as x^μ , that is:

$$a^{\mu'} = \Lambda_{\nu}^{\mu} a^\nu$$

Using the same coefficient Λ_{ν}^{μ} . For each of these (inverse) four vectors, we introduce a covariant four vector a_μ by changing the sign of its spatial component

$$a_\mu = g_{\mu\nu} a^\nu$$

Of course, we can also reverse from co empty to inverse by changing the symbol again:

$$a^\mu = g_{\mu\nu} a_\nu$$

Technically, this $g^{\mu\nu}$ is the element of a matrix g^{-1} (however, since our metric is its own inverse, $g^{\mu\nu}$ and $g_{\mu\nu}$ are the same). Given any two four vectors, a^μ and b^μ :

$$a^\mu b_\mu = a_\mu b^\mu = a^0 b^0 - a^1 b^1 - a^2 b^2 - a^3 b^3$$

It is invariant (with the same value in any inertial frame). We will call it the scalar product of a and b : this is the four-dimensional analogue corresponding to the dot product of two three vectors (a four-dimensional analogue without cross product).

If you don't want to write subscripts, you can use dot product instead. Position vector dot product:

$$\vec{x} \cdot \vec{x} = x^i x_i = \delta_{ij} x^i x^j = \begin{pmatrix} x & y \end{pmatrix} \begin{pmatrix} x \\ y \end{pmatrix} = x^2 + y^2$$

Denoted Λ as Lorentz transformation matrix:

$$S^2 = x^\mu x_\mu = g_{\mu\nu} x^\mu x^\nu = g_{\rho\sigma} x^\rho x^\sigma$$

$$S'^2 = x'^\mu x'_\mu = g_{\mu\nu} x'^\mu x'^\nu = g_{\mu\nu} \Lambda^\mu_\rho x^\rho \Lambda^\nu_\sigma x^\sigma$$

The transformation that satisfies the following conditions is called Lorentz transformation:

$$S^2 = S'^2 \Rightarrow g_{\rho\sigma} = g_{\mu\nu} \Lambda^\mu_\rho \Lambda^\nu_\sigma$$

So, it can be written as:

$$g_{\rho\sigma} = g_{\mu\nu} \Lambda^\mu_\rho \Lambda^\nu_\sigma = \left(\Lambda^T \right)_\rho^\mu g_{\mu\nu} \Lambda^\nu_\sigma$$

It can be written in the form of a matrix:

$$\Lambda^T g \Lambda = g = \begin{pmatrix} -1 & & & \\ & -1 & & \\ & & -1 & \\ & & & -1 \end{pmatrix}$$

The transformation matrix form is as follows:

$$\begin{pmatrix} 1 & & & \\ & 1 & & \\ & & \cos \theta_x & -\sin \theta_x \\ & & \sin \theta_x & \cos \theta_x \end{pmatrix}, \begin{pmatrix} 1 & & & \\ & \cos \theta_y & & \sin \theta_y \\ & & 1 & \\ & -\sin \theta_y & & \cos \theta_y \end{pmatrix}$$

$$\begin{pmatrix} 1 & & & \\ & \cos \theta_z & -\sin \theta_z & \\ & -\sin \theta_z & \cos \theta_z & \\ & & & 1 \end{pmatrix}, \begin{pmatrix} \cosh Y_x & -\sinh Y_x & & \\ -\sinh Y_x & \cosh Y_x & & \\ & & & 1 \\ & & & 1 \end{pmatrix}$$

$$\begin{pmatrix} \cosh Y_y & -\sinh Y_y & & \\ & 1 & & \\ -\sinh Y_y & \cosh Y_y & & \\ & & & 1 \end{pmatrix}, \begin{pmatrix} \cosh Y_z & -\sinh Y_z & & \\ & 1 & & \\ & & 1 & \\ -\sinh Y_z & & & \cosh Y_z \end{pmatrix}$$

therefore

$$\cosh Y_x = \frac{1}{\sqrt{1-v^2}}, \quad \sinh Y_x = \frac{v}{\sqrt{1-v^2}}$$

Obtain transformation:

$$x \rightarrow \Lambda^{-1}x = \frac{x+vt}{\sqrt{1-v^2}}, \quad t \rightarrow \Lambda^{-1}t = \frac{t+vx}{\sqrt{1-v^2}},$$

Equivalent to:

$$x \rightarrow x+vt, t \rightarrow t'$$

The Lorentz inverse transform satisfies the form:

$$x'^{\mu} = \Lambda_{\nu}^{\mu} x^{\nu}, \quad x^{\nu} = (\Lambda^{-1})_{\gamma}^{\nu} x'^{\gamma}$$

Orthogonality

$$\begin{aligned} x'^{\mu} &= \Lambda_{\nu}^{\mu} x^{\nu} = \Lambda_{\nu}^{\mu} (\Lambda^{-1})_{\gamma}^{\nu} x'^{\gamma} = \delta_{\gamma}^{\mu} x'^{\gamma}, \Lambda_{\nu}^{\mu} (\Lambda^{-1})_{\gamma}^{\nu} = \delta_{\gamma}^{\mu} \\ g_{\rho\sigma} (\Lambda^{-1})_{\tau}^{\rho} &= g_{\mu\nu} \Lambda_{\rho}^{\mu} \Lambda_{\sigma}^{\nu} (\Lambda^{-1})_{\tau}^{\rho} = g_{\mu\nu} \Lambda_{\sigma}^{\nu} \delta_{\tau}^{\mu} = g_{\tau\nu} \Lambda_{\sigma}^{\nu} \\ g^{\gamma\sigma} g_{\gamma\sigma} (\Lambda^{-1})_{\tau}^{\rho} &= \delta_{\rho}^{\tau} (\Lambda^{-1})_{\tau}^{\rho} = g^{\gamma\sigma} g_{\gamma\sigma} \Lambda_{\sigma}^{\nu} \Rightarrow (\Lambda^{-1})_{\tau}^{\gamma} g^{\gamma\sigma} g_{\gamma\sigma} \Lambda_{\sigma}^{\nu} \\ x'^{\mu} &= g_{\mu\nu} x'^{\nu} = g^{\mu\nu} x_{\rho} \Lambda_{\nu}^{\rho} = g^{\mu\nu} \Lambda_{\nu}^{\rho} g_{\mu\nu} x^{\sigma} = (\Lambda^{-1})_{\sigma}^{\mu} x^{\sigma}, \phi(x') \rightarrow \phi(x) \\ V^{\mu}(x) &\rightarrow \Lambda_{\nu}^{\mu} V^{\nu}(x) = \Lambda_{\nu}^{\mu} V^{\nu}(\Lambda^{-1}x) \end{aligned}$$

Classify all four vectors by symbol:

$$\Lambda^{\mu} V_{\mu} \begin{cases} > 0, \text{timelike} \\ < 0, \text{spacelike} \\ = 0, \text{lightlike} \end{cases}$$

Starting from vectors, we arrive at tensors in a short step: a second-order tensor $s^{\mu\nu}$ carrying two indicators, there are $4^2 = 16$ components, and two transformations Λ :

$$s'^{\mu\nu} = \Lambda_{\kappa}^{\mu} \Lambda_{\sigma}^{\nu} s^{k\sigma}$$

A third-order tensor $t^{\mu\nu\lambda}$ carries three indicators, there are $4^3 = 64$ components, and is transformed using three transformations Λ :

$$t'^{\mu\nu\lambda} = \Lambda_{\kappa}^{\mu} \Lambda_{\sigma}^{\nu} \Lambda_{\tau}^{\lambda} t^{k\sigma\tau}$$

In these hierarchies, vectors are tensors of order 1, and scalars (invariant) are

tensors of order 0. We construct covariant and "mixed" tensors by reducing the indicators (at the cost of adding a negative sign to each spatial indicator), for example

$$s_v^\mu = g_{v\lambda} s^{\mu\lambda}; s_{\mu\nu} = g_{\mu\kappa} g_{v\lambda} s^{\kappa\lambda}$$

Note that the product of two tensors itself is also a tensor: $(a^\mu b^\nu)$ is a second-order tensor; $(a^\mu t^{\nu\lambda\sigma})$ is a fourth-order tensor; wait. Finally, we can "shrink" any $n+2$ order tensor into an n -order tensor by summing a pair of upper and lower indices. Therefore, s_μ^μ is a scalar; $t_v^{\mu\nu}$ is a vector; $a_\mu t^{\mu\nu\lambda}$ is a second-order tensor.

Relativity says a moving clock (your watch) slows down compared to the ground clock, and so do bodily functions and mental processes. Specifically, when the "ground" time experiences an infinitesimal interval dt , your own (or proper) time experiences a small amount $d\tau$:

$$d\tau = \frac{dt}{\gamma} \quad (1)$$

Of course, at usual speeds, γ is close to 1, making dt and $d\tau$ almost equal. However, in elementary particle physics, the difference between laboratory time (the reading of the wall clock) and particle time (as if there were a watch on the particle) is crucial. Although we can always use equation (1) to obtain one from the other, it is usually most convenient to use proper time in practice because τ is invariant—all observers can read the particle's watch, and at any given moment, they should all be the same, even if their own clocks may differ from it and from each other.

When we talk about the "velocity" of a particle (relative to the laboratory), we mean the distance it travels (measured in the laboratory frame) divided by the time it takes (measured by the laboratory clock):

$$v = \frac{dx}{dt} \quad (2)$$

However, it is useful to introduce the proper velocity η , which is the distance traveled (also measured in the laboratory frame) divided by the proper time:

$$\eta = \frac{dx}{d\tau} \quad (3)$$

According to equation (3.29), the two velocities are related by the factor γ :

$$\eta = \gamma v \quad (4)$$

η is easier to handle because if we want to transform from the laboratory frame S to the moving frame S' , both the numerator and the denominator in equation (2) must be

transformed—leading to the cumbersome velocity addition rule in equation—while in equation (3), only the numerator needs to be transformed; $d\tau$ is invariant. In fact, the proper velocity is part of a four-vector:

$$\eta^\mu = \frac{dx^\mu}{d\tau} \quad (5)$$

its zero component is

$$\eta^0 = \frac{dx^0}{d\tau} = \frac{d(ct)}{(1/\gamma)dt} = \gamma c \quad (6)$$

thus,

$$\eta^\mu = \gamma (c, v_x, v_y, v_z) \quad (7)$$

Incidentally, $\eta_\mu \eta^\mu$ should be invariant, and it is

$$\eta_\mu \eta^\mu = \gamma^2 (c^2 - v_x^2 - v_y^2 - v_z^2) = \gamma^2 c^2 (1 - v^2/c^2) = c^2 \quad (8)$$

they do not create more invariants.

Classically, momentum is mv . In the relativistic case, we need to choose between ordinary and proper velocity. Since they're equal non - relativistically, classical ideas don't help. Defining momentum as mv breaks the consistency of momentum conservation with the relativity principle across inertial frames, while $m\eta$ preserves it. Experiments determine if momentum is conserved, but for relativistic generalization, $m\eta$ is a better choice than mv .

The conclusion is that in relativity, momentum is defined as mass times proper velocity:

$$p = m\eta \quad (9)$$

since proper velocity is part of a four-vector, momentum is also

$$p^\mu = m\eta^\mu \quad (10)$$

the spatial components of p constitute the (relativistic) momentum three-vector:

$$p = \gamma mv = \frac{mv}{\sqrt{1 - v^2/c^2}} \quad (11)$$

at the same time, the "time" component is

$$p^0 = \gamma mc \quad (12)$$

For reasons that will soon become apparent, we define the relativistic energy E as

$$E \equiv \gamma mc^2 = \frac{mc^2}{\sqrt{1 - v^2/c^2}}$$

(13)

The 0-component of p^μ is therefore E/c . Thus, energy and momentum together form a four-vector—the energy-momentum four-vector (or four-momentum)

$$p^\mu = \left(\frac{E}{c}, p_x, p_y, p_z \right) \quad (14)$$

incidentally, from equations (8) and (10), we have

$$p_\mu p^\mu = \frac{E^2}{c^2} - p^2 = m^2 c^2 \quad (15)$$

which is also completely invariant.

The relativistic momentum [equation (9)] reduces to the classical expression in the non-relativistic region ($v \ll c$), but the same cannot be said for the relativistic energy [equation (13)]. To see how this quantity is called "energy," we expand the square root in a Taylor series:

$$E = mc^2 \left(1 + \frac{1}{2} \frac{v^2}{c^2} + \frac{3}{8} \frac{v^4}{c^4} + \dots \right) = mc^2 + \frac{1}{2} mv^2 + \frac{3}{8} m \frac{v^4}{c^2} + \dots \quad (16)$$

note that the second term here is precisely the classical kinetic energy term, and the leading term mc^2 is a constant. In this sense, the relativistic formula is consistent with the classical one when the higher-order terms in the expansion at the limit $v \ll c$ can be neglected. The constant term left over at $v=0$ is called the rest energy:

$$R \equiv mc^2 \quad (17)$$

the remaining part is the energy of a moving particle called relativistic kinetic energy:

$$T \equiv mc^2 (\gamma - 1) = \frac{1}{2} mv^2 + \frac{3}{8} m \frac{v^4}{c^2} + \dots \quad (18)$$

In classical mechanics, there are no massless particles; their momentum (mv) would be zero, and their kinetic energy $\frac{1}{2} mv^2$ would be zero because $F=ma$ they would not be subject to any force. At first glance, the same might seem true in relativity, but a careful look at the formulae

$$p = \frac{mv}{\sqrt{1-v^2/c^2}}, E = \frac{mc^2}{\sqrt{1-v^2/c^2}} \quad (19)$$

when $m=0$, the numerator is zero; but if $v=c$, the denominator is also zero, and these equations become indeterminate ($0/0$). Therefore, we might allow $m=0$, provided that

the particle always moves at the speed of light. In this case, equation (19) would not serve as the definition of E and p ; however, equation (15) still holds:

$$v = c, \quad E = |p|c \text{ (for massless particles)} \quad (20)$$

if it weren't for the existence of massless particles (photons) with known facts in nature, which do indeed travel at the speed of light and their energy and momentum are indeed linked through equation (20). If equation (19) cannot define p and E , quantum mechanics provides an answer in the form of Planck's formula:

$$E = h\nu \quad (21)$$

5. Tight-binding Approximation and Second Quantization Representation

5.1 Tight-binding Approximation

Starting from the Vanier function, it is easy to derive the tight binding approximation energy band formula. When the atomic spacing of the crystal is large, it is reasonable to approximately replace the Vanier function $a_n(r-l)$ with the atomic orbital function $\phi_n(r-l)$ on the lattice point l . at this time, the tight binding approximation energy band electron wave function

$$\psi_{nk}(r) = \frac{1}{\sqrt{N}} \sum_l e^{ik \cdot l} \phi_n(r-l) \quad (22)$$

assuming that the atomic orbital functions on different lattice points are approximately orthogonal:

$$\int \phi_n^*(r-l) \phi_n(r-l') dr \approx \delta_{ll'} \quad (23)$$

using equation $\int \phi_n^*(r-l) H \phi_n(r-l') dr = \delta_{ll'} \varepsilon_n(l'-l)$, the matrix element of the wanier function of H is approximated as:

$$\begin{aligned} H_{nn}(l, l') &= \int \phi_n^*(r) H \phi_n(r-l') dr \\ &= \varepsilon_n(l'-l) \end{aligned} \quad (24)$$

substituting into $E(k) = \sum_l e^{-ik \cdot l} \varepsilon_n(l)$ and calculating up to the nearest neighbors of $\varepsilon_n(l'-l)$, we obtain:

$$\begin{aligned}
E_n(k) &= \sum_{(l'-l)} e^{ik \cdot (l'-l)} \varepsilon_n(l'-l) \\
&= \varepsilon_n(0) + \sum_{\rho} \varepsilon_n(\rho) e^{ik \cdot \rho}
\end{aligned}
\tag{25}$$

ρ represents the vector connecting the nearest neighbor lattice points $(l'-l)$, and the summation over ρ includes Z vectors, where Z is the coordination number of the lattice. Since the atomic orbital functions are known and satisfy the equation:

$$\left. \begin{aligned}
H_0 \phi_n(r-l) &= E_n^a \phi_n(r-l) \\
H_0 &= -\frac{\hbar^2}{2m} \nabla^2 + v_a(r-l)
\end{aligned} \right\}
\tag{26}$$

where E_n^a is the atomic energy level, which is also a known quantity, both $\varepsilon_n(0)$ and $\varepsilon_n(\rho)$ can be specifically calculated. Applying equations (26) and (23), we get:

$$\begin{aligned}
\varepsilon_n(0) &= \int \phi_n^*(r) H \phi_n(r-l) dr \\
&= E_n^a - A_n
\end{aligned}
\tag{27}$$

where

$$A_n = - \int \phi_n^*(r) [V(r) - v_a(r-l)] \phi_n(r-l) dr$$

represents the energy level shift of E_n^a caused by the potential of $N-1$ atoms outside the l lattice point in the lattice. Similarly

$$\begin{aligned}
\varepsilon_n(\rho) &= \int \phi_n^*(r) H \phi_n(r-\rho) dr \\
&= \int \phi_n^*(r) [V(r) - v_a(r)] \phi_n(r-\rho) dr \\
&= -J_n
\end{aligned}
\tag{28}$$

$\varepsilon_n(\rho)$ is negative, indicating that the potential fields of $(N-1)$ other atoms will transfer the bound electrons on the l lattice point to the nearest neighbor lattice point. For the sake of symmetry, let $\varepsilon_n(\rho)$ of Z nearest neighbor lattice points be the same and denoted by $-J_n$, J_n is called the overlap integral. Thus, the well-known tight binding approximate energy band formula is obtained

$$E_n(k) = E_n^a - A_n - J_n \sum_{\rho} e^{ik \cdot \rho} \quad (29)$$

when the lattice has a center of symmetry, The contribution of a pair of lattices with opposite orientations in the summation term of ρ is $-2J_n \cos(k \cdot \rho)$. Since the cosine term is between -1 and +1, the half width of the tight binding approximation energy band described in equation (9) is $2J_n$, the band center is at $E_n^a - A_n$, and the band index is marked by the quantum number of atomic energy levels, such as 3s, 3p and 3d energy bands. In the specific calculation, the periodic field $V(r)$ is represented by the superposition of atomic potential field $v_a(r-l)$

$$V(r) = \sum_l v_a(r-l) \quad (30)$$

the overlap integral is then written as:

$$J_n = - \sum_{l' \neq 0} \int \phi_n^*(r) v_a(r-l') \phi_n(r-\rho) dr \quad (31)$$

here, two-center and three-center integrals are involved. It should also be noted that the linear combination of atomic orbitals assumed in equation (22) is only applicable to non-degenerate atomic energy levels.

For the p and d orbital electrons of an atom, it belongs to the degenerate case of atomic energy levels. In this case, the tight binding approximation wave function should be extended, and the following trial functions for a given k are formed by taking into account the linear combination of each degenerate orbital ϕ_n

$$\begin{aligned} \psi_k(r) &= \sum_m C_m \phi_{mk}(r) \\ &= \frac{1}{\sqrt{N}} \sum_l \sum_m e^{ik \cdot l} C_m \phi_m(r-l) \end{aligned} \quad (32)$$

using C_m as variational parameters, for the single-electron energy, we have:

$$\left. \begin{aligned} E(k) &= \langle \psi_k | H | \psi_k \rangle = \sum_m \sum_{m'} C_m^* C_{m'} \langle \psi_{mk} | H | \psi_{m'k} \rangle \\ \sum_m |C_m|^2 &= 1 \end{aligned} \right\}$$

(33)

by finding the variational extremum, it is easy to obtain the secular equation for determining the energy bands:

$$\det \| H_{mm'}(k') - \delta_{mm'} E(k) \| = 0 \quad (34)$$

where

$$\begin{aligned} H_{mm'}(k') &= \langle \psi_{mk} | H | \psi_{m'k} \rangle \\ &= \frac{1}{N} \sum_l \sum_{l'} e^{ik \cdot (l-l')} H_{mm'}(l, l') \end{aligned} \quad (35)$$

$$H_{mm'}(l, l') = \int \phi_m^*(r-l) H \phi_{m'}(r-l') dr \quad (36)$$

unlike the H matrix element formula $\int a_n^*(r-l) H a_{n'}(r-l') dr = \delta_{nn'} \varepsilon_n(l'-l)$ of the wanier function, the matrix element formula (36) is off diagonal for m because the m and m' orbitals are degenerate. For the p orbitals, ϕ_m should be calculated as $xf(r)$, $yf(r)$, and $zf(r)$ degenerate states, and for d orbitals, it involves the determinant composed of the five degenerate states $xyf(r)$, $xzf(r)$, $yzf(r)$, $(3x^2 - r^2)f(r)$ and $(x^2 - y^2)f(r)$.

If the orbital hybridization effect is further considered, the summation over m in equation (32) should also include the interacting atomic orbitals, At this time, ψ_k is extended to the trial function of atomic orbital superposition with different symmetries, such as the superposition of s and p orbitals.

The key to the tight-binding approximation method is the linear combination of atomic orbital functions, which is often referred to as the linear combination of atomic orbitals (LCAO) method in the literature. The difficulty of this method is that the calculation of matrix elements often involves multicenter integrals, which has been greatly improved in recent years. At present, the tight-binding approximation (or LCAO) method has developed into an effective tool for the quantitative calculation of the properties of insulators, compounds, and some semiconductors.

5.2 Second Quantization Representation of the Tight-binding Approximation Hamiltonian

In narrow-band problems, electrons mainly perform localized orbital motions around the lattice points, and they have a very small probability of moving from one lattice point to another (delocalized electron motion). In this case, the tight-binding approximation method is very convenient for band calculations. Moreover, the tight-binding approximation method is not only applicable to single-electron problems but is also an effective tool for many-body problems related to narrow bands. For example, based on the tight-binding approximation, the interaction between electrons can be taken into account to discuss the band magnetism of transition metal d electrons. If the effect of lattice vibrations is considered, it involves the motion of polarons in ionic crystals, which are important research topics in solid theory.

To discuss many-body problems, the tight-binding approximation Hamiltonian in the Wannier representation should be written. As a starting point of the problem, this section only discusses the non-interacting electron system in a rigid lattice and, for simplicity, limits the discussion to single-band problems where the energy spectrum is independent of the spin orientation. At this time, the band index n and spin index σ can be omitted. The state vector formula $\psi(r) = \sum_{n,l} C_{nl} a_n(r-l)$ can be simply denoted as:

$$\psi(r) = \sum_l C_l a(r-l) \quad (37)$$

for the interaction between a rigid lattice (i.e. without lattice vibration) and electrons, it can be described by a periodic potential $V(r)$, and the single-electron Hamiltonian of the system is denoted as

$$h(r) = -\frac{\hbar^2}{2m} \nabla^2 + V(r) \quad (38)$$

following the standard method, the second quantization Hamiltonian of the system is:

$$\begin{aligned} H &= \int \psi^\dagger(r) h(r) \psi(r) dr \\ &= \sum_{l,l'} C_l^\dagger C_{l'} \int a^*(r-l) h(r) a(r-l') dr \end{aligned} \quad (39)$$

according to the tight-binding approximation, the Wannier functions in the above equation are replaced by atomic orbital functions, and only the terms $l'=l$ and $l'=l+\rho$ (ρ is the potential vector between the nearest neighbor lattice points) are

calculated, obtain the tight-binding approximation expression of H :

$$H = \varepsilon(0) \sum_l \hat{n}_l - J \sum_l \sum_{\rho} C_l^+ C_{l+\rho} \quad (40)$$

where

$$\hat{n}_l \equiv C_l^+ C_l \quad (41)$$

represents the electron number operator in the Wannier representation, $\varepsilon(0)$ is the energy of the localized orbital electrons, and J is the nearest neighbor overlap integral. Equation (40) is non-diagonal, but it can be easily diagonalized using the transformation relationship between the Wannier and Bloch representations. Two equivalent transformation methods are often used in the literature.

The most direct method is to use the operator transformation formula between the two representations:

$$C_l = \frac{1}{\sqrt{N}} \sum_k e^{ik \cdot l} C_k \quad (42)$$

the orthogonal relation a of irreducible representation of

$\sum_{R_l} \exp[-i(k - k') \cdot R_l] = N \delta_{kk'}$, translational group is obtained:

$$\left. \begin{aligned} \sum_l C_l^+ C_l &= \sum_k C_k^+ C_k \\ \sum_l C_l^+ C_{l+\rho} &= \sum_k e^{ik \cdot \rho} C_k^+ C_k \end{aligned} \right\} \quad (43)$$

substitute equation (40) to diagonalize the TBA Hamiltonian:

$$H = \sum_k \left\{ \varepsilon(0) - J \sum_{\rho} e^{ik \cdot \rho} \right\} C_k^+ C_k = \sum_k E(k) \hat{n}_k \quad (44)$$

and the tight-binding approximation energy band curve can be obtained:

$$E(k) = \varepsilon(0) - J \sum_{\rho} e^{ik \cdot \rho}$$

in equation (40), $\hat{n}_k \equiv C_k^+ C_k$ represents the electron number operator of the Bloch state.

We can also use the transformation relationship between Bloch state $|n_k\rangle$ and wanier state $|n_l\rangle$ to directly average H to get $E(k)$, which is another way. According to formula $\psi_{nk}(r) = N^{-1/2} \sum_l e^{ik \cdot l} a_n(r, l)$, the transformation relationship of States is

$$|n_k\rangle = \frac{1}{\sqrt{N}} \sum_l e^{ik \cdot l} |n_l\rangle \quad (45)$$

where n_k is the occupation number of Bloch electrons in the k state, and n_l is the occupation number of electrons in the orbital localized state around the l lattice point. In the single electron approximation, the diagonal average of Bloch states for H can be obtained by direct operation

$$\begin{aligned} E(k) &= \langle 1_k | H | 1_k \rangle \\ &= \varepsilon(0) \left\{ \frac{1}{N} \sum_l \langle 1_k | C_l^+ C_l | 1_k \rangle \right\} - J \left\{ \frac{1}{N} \sum_l \sum_\rho e^{ik \cdot \rho} \langle 1_l | C_l^+ C_{l+\rho} | 1_{l+\rho} \rangle \right\} \\ &= \varepsilon(0) - J \sum_\rho e^{ik \cdot \rho} \end{aligned} \quad (46)$$

which yields the same result as the previous method. However, the latter scheme is more convenient for extending the discussion on the influence of electron-phonon interaction on the band width in narrow-band systems.

6. Hamiltonian

For bond-charge (BC) model, we consider the positive charge background (b) and the electron (e) as a system, and write their Hamiltonian sums and their interactions, respectively. In addition to electron kinetic energy, only electrostatic Coulomb interactions are considered:

$$H = H_b + H_e + H_{eb} \quad (47)$$

$$H_e = \sum_{i=1}^N \frac{P_i^2}{2m} + \frac{1}{2} e_1^2 \sum_{i=1}^N \sum_{\substack{j=1 \\ i \neq j}}^N \frac{1}{|r_i - r_j|} e^{-\mu|r_i - r_j|} \quad (48)$$

$$H_b = \frac{1}{2} e_1^2 \int d^3x \int d^3x' \frac{n(x)n(x')}{|x-x'|} e^{-\mu|x-x'|} \quad (49)$$

$$H_{eb} = -e_1^2 \sum_{i=1}^N \int d^3x \frac{n(x)}{|x-r_i|} e^{-\mu|x-r_i|} = -e_1^2 \sum_{i=1}^N \frac{N}{V} 4\pi \int dz \frac{e^{-\mu z}}{z} = -4\pi e_1^2 \frac{N^2}{V\mu^2} \quad (50)$$

The shielding factor μ is added to the equation. r_i represents the i th electronic position. x represents the background position. e is the basic charge, $e_1 = e/\sqrt{4\pi\epsilon_0}$. Since the coulomb force is a long-range force, while $N \rightarrow \infty$, $V \rightarrow \infty$, N/V remains unchanged, if the coulomb potential energy is calculated separately, H_e , H_b and H_{eb} will diverge. In physically, when increasing the volume by keeping the electron density (N/V) constant, the average electron energy H/N should be a constant. Therefore, the divergent terms in the H_e , H_b and H_{eb} should be able to cancel each other out, in order to see this, We have added an attenuation factor μ to (48), (49), and (50), after the integration L of the cube with a side length of $L \rightarrow \infty$, And then order $\mu \rightarrow 0$, this is a commonly used technique in solid state physics calculations. $e_1 n(x)$ is the charge density at background x , and $n(x) = N/V$ is a constant.

$$H_b = \frac{1}{2} e_1^2 \left(\frac{N}{V} \right)^2 \int d^3x 4\pi \int dz \frac{e^{-\mu z}}{z} = 4\pi e_1^2 \frac{N^2}{2V\mu^2} \quad (51)$$

$$H_{eb} = -e_1^2 \sum_{i=1}^N \frac{N}{V} 4\pi \int dz \frac{e^{-\mu z}}{z} = -4\pi e_1^2 \frac{N^2}{V\mu^2} \quad (52)$$

$$\sum_{i=1}^N \frac{P^2}{2m} = \sum_{l'\sigma'} \sum_{l\sigma} a_{k_l'\sigma'}^\dagger \left\langle k_l'\sigma' \left| \frac{P^2}{2m} \right| k_l\sigma \right\rangle a_{k_l\sigma} = \sum_{l\sigma} \frac{\hbar^2 k_l^2}{2m} a_{k_l\sigma}^\dagger a_{k_l\sigma} \quad (53)$$

In the above formula, use k_l representative k_{xl} , k_{yl} and k_{zl} , $l = 0, \pm 1, \pm 2, \pm 3, \dots$ for typographical convenience, we sometimes use k and k' in lieu of k_l and k_l' , just

remember the momentum k take discrete values instead of continuous values. The second item in (48) is

$$\begin{aligned} & \frac{1}{2} e_1^2 \sum_{l'\sigma'} \sum_{m'\lambda'} \sum_{l\sigma} \sum_{m\lambda} a_{k_l, \sigma'}^\dagger a_{k_m, \lambda'}^\dagger (k_l, \sigma', k_m, \lambda') \left| \frac{e^{-\mu|r_1-r_2|}}{|r_1-r_2|} \right| k_l \sigma, k_m \lambda a_{k_m \lambda} a_{k_l \sigma} \\ &= \frac{1}{2} e_1^2 \sum_{l'} \sum_{m'} \sum_{l\sigma} \sum_{m\lambda} \delta_{\sigma\sigma'} \delta_{\lambda\lambda'} a_{k_l, \sigma'}^\dagger a_{k_m, \lambda'}^\dagger (k_l, k_m) \left| \frac{e^{-\mu|r_1-r_2|}}{|r_1-r_2|} \right| k_l k_m a_{k_m} a_{k_l} \end{aligned} \quad (54)$$

The matrix elements are first calculated in the position representation. Insert two completeness relations in the matrix element in the above equation:

$$\begin{aligned} \int d^3 r^a \int d^3 r^b |r^a r^b\rangle \langle r^a r^b| &= 1 \\ \int d^3 r^\gamma \int d^3 r^\delta |r^\gamma r^\delta\rangle \langle r^\gamma r^\delta| &= 1 \end{aligned}$$

And

$$\begin{aligned} (k_l, k_m) \left| \frac{e^{-\mu|r_1-r_2|}}{|r_1-r_2|} \right| k_l k_m &= \frac{1}{V^3} \int d^3 r^a \int d^3 r^b e^{-i(k_l, -k_l) \cdot r^a} e^{-i(k_m, -k_m) \cdot r^b} \frac{e^{-\mu|r^a-r^b|}}{|r^a-r^b|} \\ &= \delta(k_l + k_m, k_l + k_m) \frac{1}{V} \int \frac{e^{-\mu r}}{r} e^{-i(k_l, -k_l) \cdot r} d^3 r \\ &= \delta(k_l + k_m, k_l + k_m) \frac{2\pi}{V} \int r e^{-\mu r} \left(\frac{2}{kr} \sin kr \right) dr \\ &= \delta(k_l + k_m, k_l + k_m) \frac{1}{V} \frac{4\pi}{(k_l - k_l)^2 + \mu^2} \end{aligned} \quad (55)$$

In the above calculation, the second step uses the independent variable substitution:

$r^a + r^b = r'$ 、 $r^a - r^b = r$ [Jacobian determinant $J = (1/2)^3$], substitute this equation

back (54), $k_l = k$, $k_m = k'$, $k_l = k + q$, $k_m = k' - q$, the second item in H_e is

$$\frac{e_1^2}{2V} \sum_k \sum_{k'} \sum_q \sum_{\sigma\lambda} \frac{4\pi}{q^2 + \mu^2} a_{k+q, \sigma}^\dagger a_{k'-q, \lambda}^\dagger a_{k' \lambda} a_{k \sigma} \quad (56)$$

Separate out $q = 0$ is

$$\frac{e_1^2}{2V} \sum_k \sum_{k'} \sum_q \sum_{\sigma\lambda} \frac{4\pi}{\mu^2} a_{k\sigma}^\dagger a_{k'\lambda}^\dagger a_{k' \lambda} a_{k \sigma} = \frac{e_1^2}{2V} \frac{4\pi}{\mu^2} (N^2 - N)$$

N is the total number of particles, because

$$a_{k\sigma}^\dagger a_{k'\lambda}^\dagger a_{k'\lambda} a_{k\sigma} = N_{k\sigma} N_{k'\lambda} - N_{k\sigma} \delta_{kk'} \delta_{\sigma\lambda}$$

Now substitute (53) and (56) back to equation (48), H_e is

$$H_e = \sum_{k\sigma} \frac{\hbar^2 k^2}{2m} a_{k\sigma}^\dagger a_{k\sigma} + \frac{e_1^2}{2V} \sum_q^* \sum_{k\sigma} \sum_{k'\lambda} \frac{4\pi}{q^2 + \mu^2} a_{k+q,\sigma}^\dagger a_{k'-q,\lambda}^\dagger a_{k'\lambda} a_{k\sigma} + \frac{e_1^2}{2V} \frac{4\pi}{\mu^2} (N^2 - N) \quad (57)$$

In the formula, the q on the sum sign of "*" indicates that the part where $q=0$ is ignored during the sum. When $V \rightarrow \infty, N \rightarrow \infty$, while keeping N/V constant, the last term to the right of the equal sign causes the average energy H_e/N of each particle to become:

$$\frac{1}{2} 4\pi e_1^2 \left(\frac{N}{V} \right) \frac{1}{\mu^2} - \frac{1}{2} 4\pi e_1^2 \left(\frac{N}{V} \right) \frac{1}{N} \frac{1}{\mu^2}$$

The former term is constant, and the latter term tends to zero. If $\mu \rightarrow 0$, the former term becomes a divergent term. However, this term just cancels out the divergent H_b and H_{cb} term. Thus, the Hamiltonian of the system becomes

$$H = \sum_{k\sigma} \frac{\hbar^2 k^2}{2m} a_{k\sigma}^\dagger a_{k\sigma} + \frac{e_1^2}{2V} \sum_q \sum_{k'} \sum_{\sigma\lambda} \frac{4\pi}{q^2} a_{k+q,\sigma}^\dagger a_{k'-q,\lambda}^\dagger a_{k'\lambda} a_{k\sigma} = H_0 + H_1 \quad (58)$$

7. Energy level

7.1 Establishment of the Hamiltonian operator

In a multi electron atom, the kinetic energy operator of the i -th electron is $-\frac{\hbar^2}{2m_e} \nabla_i^2$, its potential energy in the average potential field $V(r_i)$ generated by the nucleus and other $(Z-1)$ electrons is $V(r_i)$. Then the Hamiltonian operator of the whole atom is

$$\hat{H} = \sum_{i=1}^Z \left[-\frac{\hbar^2}{2m_e} \nabla_i^2 + V(r_i) \right].$$

7.2 Separating variables and single electron equation

Let the wave function $\Psi \left(\vec{r}_1, \vec{r}_2, \dots, \vec{r}_Z \right) = \psi_1 \left(\vec{r}_1 \right) \psi_2 \left(\vec{r}_2 \right) \dots \psi_Z \left(\vec{r}_Z \right)$ be substituted into the time-dependent Schrodinger equation $i\hbar \frac{\partial \Psi}{\partial t} = \hat{H} \Psi$ to obtain

$$i\hbar \frac{\partial \Psi}{\partial t} = \sum_{i=1}^Z \left[-\frac{\hbar^2}{2m_e} \nabla_i^2 + V(r_i) \right] \Psi \quad (59)$$

Since $\Psi(\vec{r}_1, \vec{r}_2, \dots, \vec{r}_Z) = \psi_1(\vec{r}_1) \psi_2(\vec{r}_2) \cdots \psi_Z(\vec{r}_Z)$, then

$$i\hbar \frac{\partial \Psi}{\partial t} = \sum_{i=1}^Z \left[-\frac{\hbar^2}{2m_e} \nabla_i^2 + V(r_i) \right] \psi_1(\vec{r}_1) \psi_2(\vec{r}_2) \cdots \psi_Z(\vec{r}_Z) \quad (60)$$

After separating the variables, the steady-state Schrodinger equation of the single electron is obtained as

$$\left[-\frac{\hbar^2}{2m_e} \nabla_i^2 + V(r_i) \right] \psi_i(\vec{r}_i) = E_i \psi_i(\vec{r}_i) \quad (61)$$

7.3 Equation representation in spherical coordinate system

For spherically symmetric potential energy $V(r_i)$, $\psi_i(\vec{r}_i)$ is represented as

$\psi_i(\vec{r}_i) = R_{nl}(r) Y_{lm}(\theta, \varphi)$ in the spherical coordinate system.

The single electron steady state Schrodinger equation in spherical coordinates is

$$\left[-\frac{\hbar^2}{2m_e} \left(\frac{1}{r^2} \frac{\partial}{\partial r} \left(r^2 \frac{\partial}{\partial r} \right) + \frac{1}{r^2 \sin \theta} \frac{\partial}{\partial \theta} \left(\sin \theta \frac{\partial}{\partial \theta} \right) + \frac{1}{r^2 \sin^2 \theta} \frac{\partial^2}{\partial \varphi^2} \right) + V(r) \right] \psi_i(\vec{r}_i) = E_i \psi_i(\vec{r}_i) \quad (62)$$

Substitute $\psi_i(\vec{r}_i) = R_{nl}(r) Y_{lm}(\theta, \varphi)$ into **Eq(62)**, and separate the variables to obtain the angular equation and radial equation as

$$\left[-\frac{\hbar^2}{2m_e} \frac{1}{r^2} \frac{d}{dr} \left(r^2 \frac{dR_{nl}(r)}{dr} \right) + V(r) R_{nl}(r) \right] + \frac{l(l+1)\hbar^2}{2m_e r^2} R_{nl}(r) = E_{nl} R_{nl}(r) \quad (63)$$

The solution of the angular equation is spherical harmonic function $Y_{lm}(\theta, \varphi)$, which is determined by the quantum numbers l and m .

7.4 Introduction of effective potential energy and solution

To solve the radial equation, the effective potential energy $V_{eff}(r) = V(r) + \frac{l(l+1)\hbar^2}{2m_e r^2}$ is introduced, and the radial equation becomes

$$-\frac{\hbar^2}{2m_e} \frac{1}{r^2} \frac{d}{dr} \left(r^2 \frac{dR_{nl}(r)}{dr} \right) + V_{eff}(r) R_{nl}(r) = E_{nl} R_{nl}(r) \quad (64)$$

For the solution of **Eq(64)**, combined with the boundary conditions, when $r \rightarrow 0$, $R_{nl}(r)$ is finite; When $r \rightarrow \infty$, $R_{nl}(r) \rightarrow 0$, the expression of the energy eigenvalue E_{nl} related to the principal quantum number n and the angular quantum number l can be obtained.

7.5 Formula for determining effective nuclear charge number and energy level

Using the central force field approximation, $V(r)$ is approximated to $V(r) = -\frac{Z^* e^2}{4\pi\epsilon_0 r}$,

where $Z^* = Z - \sigma$ and σ are shielding constants, which can be determined by the slay rule, etc.

By substituting $V(r) = -\frac{Z^* e^2}{4\pi\epsilon_0 r}$ into the expression of energy eigenvalue obtained by

solving the radial equation **Eq(64)**, the energy level formula $E_{n,l} = -\frac{m_e (Z^* e^2)^2}{8\epsilon_0^2 \hbar^2 n^2} = -\frac{R_H Z^{*2}}{n^2}$

of multi electron atom can be obtained, where $R_H = \frac{m_e e^4}{8\epsilon_0^2 \hbar^2}$ is the Rydberg constant.